Nanostructured All-cellulose Membranes for Efficient Ultrafiltration of Wastewater

Mengying Yang[1], Sarah Lotfikatouli[2,4], Yvonne Chen[1], Tony Li[1],

Hongyang Ma[1,3], Xinwei Mao[2,4] and Benjamin S. Hsiao[1*]

[1] Department of Chemistry, Stony Brook University, Stony Brook, NY 11794, USA

[2] Department of Civil Engineering, Stony Brook, NY 11794, USA

[3] State Key Laboratory of Organic-Inorganic Composites, Beijing University of Chemical Technology, Beijing 100029, China

[4] New York State Center for Clean Water Technology, Stony Brook, NY 11794

[*]Corresponding Author: Tel: +1(631)632-7793, Fax: +1(631)632-6518, E-mail: Benjamin.Hsiao@stonybrook.edu

Abstract

One major challenge in utilization of ultrafiltration (UF) membrane for wastewater treatment is its inevitable tendency of biofouling (from biomolecules to microorganisms). To overcome this challenge, nanostructured cellulose membranes with hydrophilic surface and high porosity (~80% without pressurization) was demonstrated in this study. The cellulose membrane consisted of a lyocell microfiber scaffold infused with cellulose nanofibers (CNF), crosslinked with polyamideamine-epichlorohydrin (PAE). The demonstrated membranes showed good mechanical strength (wet stress: 3.5 - 8.0 MPa), pH resistance (pH 2.5 - 9.0) and stability in hot water (60 ºC). The optimized cellulose membrane exhibited high permeation flux (127.6 ± 21.8 L m^{-2} h^{-1} bar^{-1}), excellent separation efficiency (> 99.9%), good flux recovery ratio (> 95%) and self-healing ability for wastewater filtration, compared with commercial polymeric membranes (e.g., polyvinylidene difluoride (PVDF) and polyether sulfone (PES)). The resistance-in-series and three combined cake-filtration models were applied to investigate the fouling behavior of the cellulose and PVDF/PES UF membranes. While all membranes suffered cake layer precipitation and pore blocking issues, the cellulose membranes exhibited near total recyclability upon washing due to the hydrophilic and negatively charged CNF membrane surface. This study illustrated the promising potential of using cellulose membranes for high-efficient wastewater treatment and its superior antifouling performance compared to existing commercial membranes.

Keyword: Cellulose, Ultrafiltration Membrane, Porosity, Fouling, Wastewater

1. Introduction

Wastewater treatment is crucial for protecting aquatic, air and soil environments as well as for ensuring the human and animal health. However, due to the complex circumstances in different wastewater sources and the relatively high cost of the treatment system, wastewater treatment has not been fully adopted around the world, especially in the rural communities of the underdeveloped countries [1, 2]. In the past decades, a multitude of water purification technologies, including coagulation and flocculation, catalytic and photocatalytic oxidation [3], chemical adsorption and precipitation [2, 4] and membrane separation have been advanced, leading to developments of many high efficiency and small footprint water purification systems with benign environmental impact and low energy/capital costs for varying applications [5, 6]. Nonetheless, for wastewater treatment, the essential process of membrane filtration still needs advancement to overcome the fouling and sustainability issues. Commercialized membranes for wastewater treatment are mainly made of synthetic polymers, including polyvinylidene fluoride (PVDF), polyethersulfone (PES), polysulfone (PS) and polyacrylonitrilic (PAN). While they possess good mechanical properties, controllable pore size and distribution, and good reproducibility [6, 7], they are hydrophobic and susceptible to fouling. The issue of membrane fouling in the treatment system requires frequent maintenance, thus greatly increasing the operational cost [8]. Moreover, the synthetic polymer membranes cannot be easily degraded in the environment, whereas the disposal of the used membranes can cause further environmental problems [9, 10].

To deal with the above challenges (i.e., membrane fouling and disposal of used membrane), our group has been exploring the replacement of synthetic polymers with nature polymers, such

as cellulose, for manufacturing of filtration membranes. This is because cellulose is the most abundant natural polymer on Earth, and can be obtained from many biomass sources, such as woods, agricultural residues, vascular plants, aquatic plants, and bacteria [11]. The intrinsic properties of cellulose, such as hydrophilicity, non-toxicity, water stability, sustainability and good mechanical properties, are suitable for water purification applications [12, 13]. In addition, the modifications of cellulose surface can further render it into functional scaffolds for applications such as sorption, flocculation, catalytic degradation, disinfection, and membrane filtration [14, 15]. The recent advances of extracting nanoscale materials from cellulose (nanocellulose) have further enhance the efficiency of water remediation capability due to the increased surface area and functionality. These nanomaterials, such as cellulose nanocrystals (CNC) and cellulose nanofibers (CNF), have shown great potential to improve the membrane properties [15]. In specific, some recent studies showed that the inclusion of nanocellulose in ultrafiltration (UF) membranes could offer the added benefits of reduced biofouling suitable for wastewater treatment [16-19].

There have been several ways to incorporate nanocellulose into synthetic membranes, such as the use of CNC/CNF and polymer solution to produce hybrid nanocomposite membranes, impregnated CNC/CNF into an electrospun scaffold to generate hybrid nanofibrous membranes, or vacuum filtrated/solution casting on top of a polymer substrate to fabricate the thin-film nanocomposite (TFNC) membranes [15]. The major component of these composite membranes, however, is still the synthetic polymer. Recently, several research groups have demonstrated the use of cellulose membranes for water filtration such as for oil/water separation [20], dye removal [21], or heavy metal adsorption [22]. From these studies, several challenges were noted in the fabrication of cellulose membranes. First, the commonly applied vacuum-filtration strategy

usually results in a condensed structure of membrane, which renders a low permeation flux in water treatment. Second, a separate supporting membrane is essential to ensure the mechanical strength of the hierarchical cellulose membrane during the membrane preparation process, where nanocellulose is added through an additional step, such as electrospinning, additive printing, and dip coating [20, 21, 23]. Third, often organic solvents need to be used, either to dissolve cellulose for membrane casting or to immerse the membrane for post-treatment during fabrication [21, 24]. To overcome these challenges, we aim to develop a simple and low-cost method that can produce the innovative nanostructured membranes with good mechanical strength, high porosity and suitable pore size for superb filtration properties (i.e., high permeate flux and rejection ratio). We believe that it is the first completely sustainable all-cellulose UF membrane that can be prepared in one step and has superior filtration performance than most of the commercial polymer membranes.

In this study, we demonstrate a strong and highly hydrophilic nanostructured cellulose membrane system with high porosity (~ 80%) in a one-step approach without pressurization or usage of organic solvent. This membrane system consisted of a lyocell microfiber scaffold infused with TEMPO-oxidized CNF crosslinked by polyamideamine-epichlorohydrin (PAE). The infusion of cellulose nanofiber in cellulose-based microfiber avoided the potential delamination problem which is commonly seen in layer-by-layer coated membranes. The surface properties, crystallinity, zeta potential, pore size, permeability, and porosity of the cellulose membranes were carefully characterized. To compare the filtration performance, demonstrated membranes and commercially available polymeric UF membranes such as polyvinylidene difluoride (PVDF) and polyether sulfone (PES) membranes, a continuously operating wastewater filtration test was designed and

conducted. The membranes before and after fouling as well as cleaned with sodium hypochlorite (NaClO) were further characterized by Fourier-transform infrared spectroscopy (FTIR), contact angle and zeta potential techniques. The resistance-in-series models and three combined cake-filtration models were used to analyze the membrane fouling behavior. In addition, the impact of environmental conditions (e.g., pH and temperature) and physical scratch on the performance of cellulose membranes were also carried out.

2. Experimental

2.1. Materials

Untreated jute fibers were provided by Toptrans Bangladesh Ltd. in Bangladesh. Chemical reagents: 2,2,6,6-Tetramethyl-1-piperidinyloxy (TEMPO, 98%), sodium bromide (NaBr), sodium hypochlorite (NaClO, 14.5% available chlorine), phosphate buffer (0.025M, pH 2.5) and sodium bicarbonate buffer (0.05M, pH 9.0) were purchased from Fisher Scientific and were used as received. Lyocell nanofibrillated fibers with a fiber diameter between 0.1-0.5 μm were provided by Engineered Fibers Technology (EFT), LLC. Hydrophilic polyvinylidene fluoride (PVDF) membrane filter (Durapore®) with 0.65 μm pore size was purchased from Millipore Sigma Company. Polyamideamine-epichlorohydrin (PAE) resin (Kymene 920A) was purchased from Solenis, LLC. Commercial-grade PVDF-A6 (MWCO: 500 kDa, composed of neat PVDF), PVDF-V6 (MWCO: 500 kDa, composed of PVDF treated to create positive surface charge) and PES-LX

(MWCO: 300 kDa, composed of neat PES) membranes were purchased from the Sterlitech Corporation.

2.2. Preparation of Cellulose Membranes

A suspension of CNF extracted from jute fibers was prepared according to the TEMPO-oxidation protocol published in the literature [25] [18]. Cellulose membranes containing different ratios of dry mass density (g m^{-2}) were prepared using by mixing 0.5 wt% lyocell and 0.15 wt% CNF (1.60 mmol/g in degree of oxidation, average width was 4.9 ± 1.3 nm, Fig. S1*, Supporting Information*) suspensions as follows. First, the pre-weighted lyocell (50 g m^{-2} dry mass density) and CNF (0.5 – 2.5 g m^{-2} dry mass density) mixed suspension was stirred rigorously with a magnetic stirring bar for 30 min. Then, the mixed suspension was poured evenly onto a wetted hydrophilic PVDF filter membrane (average pore size: 0.65 μm) supported by a ceramic funnel and was drained via gravity filtration for 3 days until the membrane was totally dried. The cellulose membranes were labeled based on the ratio of lyocell and CNF in terms of their dry mass density. For example, 50-0.0, 50-0.5, 50-0.75, 50-0.85, and 50-2.5 membranes stand for the membranes prepared with 50 g m^{-2} lyocell and 0.0, 0.5, 0.75, 0.85 and 2.5 g m^{-2} CNF, respectively. Later, the dried membranes were peeled off from the PVDF filter, immersed in a crosslinking agent (0.1wt% PAE) for 30 min, and then cured in the oven for another 30 min at 120℃. The illustration of the crosslinking reaction (i.e., PAE-CNF crosslinking and PAE-PAE self-crosslinking) pathways and the preparation of cellulose membrane is depicted in Fig. 1a and 1b, respectively. The resulting membranes were washed with distilled water several times to remove unreacted crosslinking agent,

and then dried and stored at 50% humidity and room temperature before the tensile test. For FT-IR and XRD measurements, membrane samples were dried at 50 C° for 30 min to minimize the signals from water.

(a)

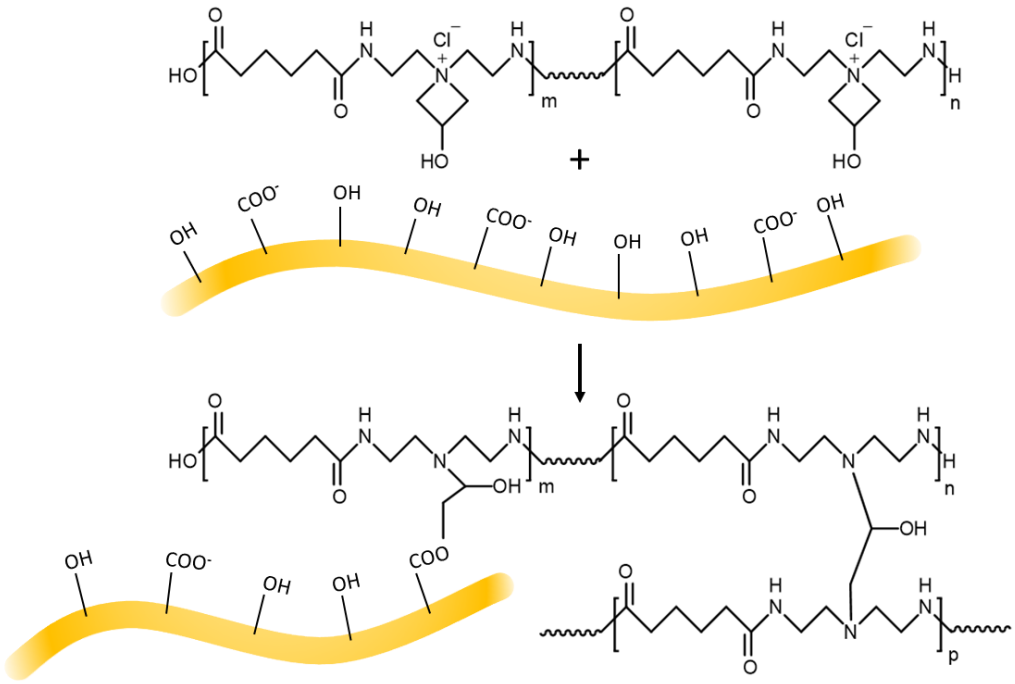

(b)

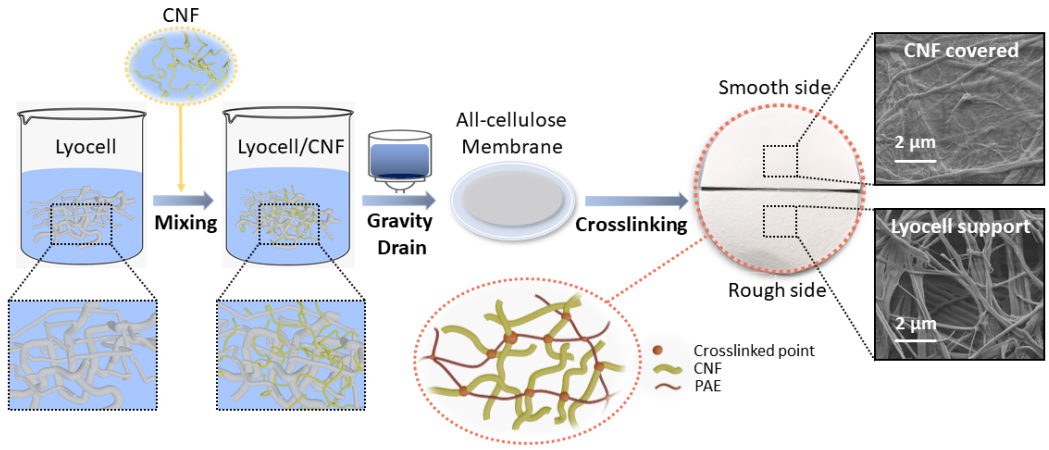

Fig. 1 The preparation scheme of all-cellulose membrane preparation and the crosslinking mechanism and enhance the substrate strength. (a) Illustration of crosslinking reaction pathway: PAE-CNF crosslinking (the yellow ribbon represents CNF) and PAE-PAE self-crosslinking. (b) Preparation of cellulose membrane; photograph and SEM images of the 50-0.85 crosslinked membrane (i.e., 50 g m^{-2} lyocell and 0.85 g m^{-2} CNF). The smooth side was the side attached to the PVDF filter and the rough side was the side exposed to air during gravity draining.

2.3. Characterization of Cellulose Membranes

The morphology of CNF was characterized by a FEI BioTwinG2 transmission electron microscope (TEM) equipped with an AMT XR-60 CCD digital camera system (Hillsboro, OR, USA). The structure of the cellulose membranes was characterized using a Thermo Nicolet iS10 FTIR spectrometer equipped with attenuated total reflection (ATR) configuration, and by a wide-angle X-ray diffraction (WAXD) instrument (Benchtop Rigaku MiniFlex 600). The zeta potentials of the lyocell, CNF, and the mixture suspensions were evaluated by a Nano Brook Series size and zeta potential analyzer (Brookhaven, Holtsville, NY, USA). The zeta potentials of the cellulose membranes and commercial PVDF and PES UF membranes were characterized by a zeta potential analyzer (Anton Paar, SurPASS 3, Graz, Austria).

The surface and cross-sectional morphologies of cellulose membranes were examined by a Schottky field emission scanning electron microscope (FE-SEM) (LEO Gemini 1550, Zeiss, Oberkochen, Germany) at an accelerating voltage of 2.5 kV. The water contact angles of the tested

membranes were determined using a Dataphysics contact angle analyzer (OCA 15EC, Hamden, CT, USA), where more than five different locations on each membrane were tested to obtain an average value. Various sizes of unfunctionalized polystyrene (PS) beads (Polybead® Microspheres, 0.05, 0.2, and 1.0 μm) were used to estimate the pore size of the cellulose membrane by the dead-end filtration cell (Amicon Stirred Cell, 50 mL). The rejection ratio of the solute having PS nanoparticles was determined by a Shimadzu total organic analyzer (TOC-VCPN, Kyoto, Japan). The tensile strength of the cellulose membranes was evaluated using a modified Instron 4442 tensile apparatus. In brief, the precut membranes strips (10 mm × 50 mm × 0.20 mm; stored at 50% humidity and 25 ºC for 24 hours for dry sample testing; immersed in water at 25 ºC for one hour for wet sample testing). The tensile samples were uniaxially stretched in a symmetric manner at a rate of 10 mm/min and room temperature. A mean tensile strength was determined by testing 10 samples. The membrane porosity (P_r) was determined by the gravimetric method defined as follows:

$$P_r(\%) = \frac{W_w - W_d}{\rho \times A \times D} \quad (1)$$

where W_w is the weight of wet membrane, W_d is the weight of dry membrane, ρ is density of distilled water (g/cm^3), A is membrane area (cm^2), and D is the thickness of wet membrane (cm).

2.4. Membrane Performance for Wastewater Treatment

To test the UF performance of the cellulose and commercial PVDF/PES membranes, activated sludge (or mixed liquor suspended solids MLSS) was collected from a membrane

bioreactor in the Riverhead Sewage Treatment Plant, Long Island, NY and used as to test the membrane performance. This MLSS was stored at 5 ˚C before the filtration experiment. The separation efficiency and antifouling properties of a chosen cellulose membrane (crosslinked 50-0.85 membrane) and commercial PVDF-V6, PVDF-A6, and PES-LX membranes were evaluated by measuring the pure water flux (J_w), water flux in the presence of effluent (J_p), retention ratio of foulant (R) and flux recovery ratio (Fr) using a dead-end UF cell (Model HP4750X, Sterlitech Corporation, USA) with an effective membrane area (A) of 14.6 cm^2. All membranes were first compacted using distilled water under 0.5 bar pressure until a stable permeation flux was reached. Subsequently, the MLSS was added into the reservoir and fully stirred to start the fouling emulation. The flux value was recorded to monitor the flux decline at different time intervals at 0.5 ± 0.02 bar and 24 ± 2˚ C. The turbidity and TDS concentrations were measured by a turbidity meter (Thermo Scientific Orion AQ3010) following the published weighing method [26]. Briefly, 20 mL weighted sample was filtered through a 0.45 μm membrane filter (Millipore Co., Bedford, MA, USA). Then, the TDS concentration (mg L^{-1}) was calculated by drying the filtrate at 105 ºC overnight and then weighing the dried solids.

The membrane permeation flux (J) was calculated using the following equation with the unit of L m^{-2} h^{-1} (LMH):

$$J = \frac{V}{(A \times t)} \quad (2)$$

where V is the volume of the permeate passing through the membrane at time t, and A is the effective membrane area. The rejection ratio (R_t) was determined by measuring the turbidity and TDS concentration in wastewater (C_0) and permeate (C_t) as follows:

$$R_t\ (\%) = (1 - \frac{C_t}{C_0}) \times 100 \quad (3)$$

The flux recovery ratio ($F_{r,w}$) was evaluated after applying either hydraulic cleaning (rinsing the membrane for 30 seconds at a flow rate of 0.6 gpm) or NaClO cleaning (i.e., immersing the membrane in 0.05 wt% NaClO solution for 30 seconds followed by three rounds of rinsing with distilled water) using the following equation:

$$F_{r,w}\ (\%) = \frac{J_{w,w}}{J_w} \times 100 \quad (4)$$

where $J_{w,w}$ is the pure water flux after hydraulic cleaning and J_w is the pure water flux prior to the membrane fouling.

2.5. Fouling Mechanism Study of Cellulose Membranes

The resistance-in-series model utilizes Darcy's Law to characterize filtration resistance [27, 28]. The formulas are shown below.

$$R_t = \frac{\Delta P}{\mu \times J_{w1}} \quad (5)$$

$$R_M = \frac{\Delta P}{\mu \times J} \quad (6)$$

$$R_M + R_P = \frac{\Delta P}{\mu \times J_{w2}} \quad (7)$$

$$R_C = R_t - (R_M + R_P) \quad (8)$$

where J is the last flux point of DI compaction, J_{w1} is the last flux point of the current wastewater run, J_{w2} is the first flux point of the next wastewater run, ΔP is transmembrane pressure, and μ is the viscosity of permeate.

This model accounts for three types of resistances (pore clogging, cake layer, and inherent membrane resistance), assigning each a quantitative variable. A fourth quantitative variable, R_f (total fouling resistance) is determined by summating the variables R_C and R_P. The percent of reversible (cake layer) and irreversible (pore clogging) fouling can be demonstrated by calculating the variables ratio R_C/R_f and R_P/R_f.

$$R_t = R_C + R_P + R_M \quad (9)$$

$$R_t = R_f + R_M \quad (10)$$

$$R_f = R_C + R_P \quad (11)$$

where R_t is total resistance, R_c is cake-layer induced resistance, R_p is pore clogging induced resistance, R_M is inherent membrane resistance and R_f is fouling resistance. We note that there is one form of external fouling (cake layer) and three forms of internal fouling (standard, complete, and intermediate pore blocking) [29]. The resistance-in-series model addresses internal fouling, but it does not specify which mechanism is dominant. As a result, this model alone is insufficient for a full analysis of the membrane fouling and a supplementary model is needed. To deal with this issue, three models: cake-filtration complete pore blocking Model (CFCBM), cake-filtration standard pore blocking model (CFSBM) and cake-filtration intermediate pore blocking model (CFIBM) were used together to analyze the internal membrane fouling data in this study (with the

Origin Pro software). [30, 31] A variety of parameters were selected for comparison to determine the model that fit best to the experimental data (the chosen combined fouling models at constant pressure to investigate the fouling mechanism are summarized in Table S1, *Supporting Information*).

2.6. Membrane Self-Healing and Stability Study

To investigate the self-healing ability of selected membranes, the filtration performance of the scratched cellulose, PVDF-V6, PES-LX, and PVDF-A6 membranes was evaluated by distilled water using the dead-end filtration system. In this test, the membrane was first compressed with distilled water at pressure of 0.5 bar until the permeate flux was stable. A blade cutter was used to create a 3 cm scratch in the middle of membranes. The flux change was monitored before and after the scratch under the same filtration conditions.

The applicable pH range and temperature resistance for the cellulose membrane was also investigated by using phosphate buffer solution (pH = 2.5), sodium bicarbonate buffer solution (pH = 9.0) and 60 ºC warm distilled water. For the pH resistance test, the cellulose membrane was pre-immersed in buffer solutions at two different pH values and room temperature for 3 days. For the temperature resistance test, the cellulose membrane was stirred in 60 ºC warm water for 7 days. After the pretreatment, all membranes were washed with water and tested via dead-end ultrafiltration protocol for MLSS as described in section 2.4.

To challenge the cellulose membrane for long-term wastewater filtration, a lab-scale immersed membrane filtration system was used (the schematic diagram of the immersed membrane module is shown in Fig. S2, *Supporting Information*). In this test, the membrane module with a total surface area of 0.0338m^2 was undergone a 6-hour water compaction at 0.5 bar. Subsequently, the compacted membrane module was placed in a sludge feed tank with a capacity of 40L. A negative pressure in the membrane module was generated by a vacuum pump, where the permeate from the wastewater was sucked through the connected channels into the collection flask. The permeate was collected continuously for 12 hours. In this test, the pressure was stabilized at 0.5 bar, where the volume of the permeate was used to calculate the flux using Equation 2.

3. Results and Discussion

3.1. Characterization of Cellulose Membranes

The cellulose membrane was first characterized to assess its surface properties, crystallinity, zeta potential, permeability, pore size and porosity. Fig. 2a shows the FT-IR spectra of the cellulose membranes prepared with different CNF dry mass ratios (0.0 – 1.0 g m^{-2}) and crosslinking conditions. It was seen that the stretching vibration at 1601 cm^{-1} of the carboxylate group from CNF was present in all crosslinked and non-crosslinked 50-1.0 (50 g m^{-2} lyocell and 1.0 g m^{-2} CNF)

membranes. Compared to the neat cellulose membranes, the introduction of PAE resulted in the appearance of two absorption bands: amide I group at 1640 cm^{-1} and amide II group at 1550 cm^{-1} [32]. Due to the adsorbed water in the membrane, the amide I band partly overlapped with the symmetric deformation vibrations of water molecules. Although PAE could self-crosslink slowly under room temperature or quickly during the heating process [33], the stretching C=O vibration of the ester bond at 1728 cm^{-1} in all 50-1.0 crosslinked membranes indicated the covalent bond linkage between the azetidinium groups of PAE and carboxyl groups of CNF, while the low peak intensity was caused by the small loading amount of CNF [34, 35].

The XRD patterns of CNF, lyocell, and cellulose membranes were displayed in Fig. 2b. The crystalline regions in CNF were represented by the diffraction peaks at 2θ = 23.1º, 16.4º, and 14.8º, representing the (200), (110), and ($1\bar{1}0$) lattice planes of the cellulose I structure, respectively [36]. While lyocell is the regenerated cellulose fibers, which showed three diffraction peaks at 2θ = 22.0º, 20.3º, and 12.3º, corresponding to the (020), (110), and ($1\bar{1}0$) lattice planes of the cellulose II structure, respectively [37]. All cellulose membranes illustrated similar diffraction patterns as that of lyocell fibers because of the small loading amount of CNF (1.0 g m^{-2}). It was seen that the crosslinking treatments did not change the crystalline structure of the cellulose I structure because the crosslinking process mainly occurred in the amorphous domains while the crystalline domains of CNF were unaffected [38, 39].

The crosslinking reaction between CNFs and PAE in the cellulose membrane could also be verified indirectly by the membrane zeta potential measurement. The zeta potential results of

non-crosslinked (No CL) and crosslinked (CL) cellulose membranes as a function of pH (in the range of pH = 5-9) are shown in Fig. 2c, where all zeta potential values were negative. In has been shown that the addition of CNF could decrease the zeta potential of the mixed Lyocell/CNF suspension because of the presence of additional carboxyl groups (Fig. S3, *Supporting Information*). However, the behavior of the zeta potential change in the cellulose membrane was found to be different due to the presence of PAE. In Fig. 2c, it was seen that the negative charge of the No CL cellulose membrane surface (50 g m^{-2} lyocell and 0.85 g m^{-2} CNF membrane) mainly came from the deprotonation of carboxyl groups on CNF, which increased slightly with the pH value resulting in the slight decrease in the membrane zeta potential. However, in the CL cellulose membrane, the deprotonation of the amino groups in PAE could also contribute to the negative zeta potential of the membrane surface, especially with the increase in pH value. This has led to a more pH-dependent zeta potential trend of the CL cellulose membrane (Fig. 2c). We note that the cationic primary amide group and azetidinium functional group of PAE have a high affinity of forming covalent bonds with the carboxyl groups on CNF, the sharp increase in the zeta potential of the CL cellulose membrane with decreased pH was due to the protonation of secondary/tertiary amino groups on PAE after the crosslinking process [40].

To investigate how the addition of CNF could influence the pore size of the cellulose membranes, a dead-end filtration test using spherical PS nanoparticles of varying sizes was conducted to determine the pore size of the cellulose membranes (Fig. 2d). It was seen when the CNF loading in the cellulose membranes increased, the corresponding pore size decreased from 1 μm for the original lyocell membrane (50-0) to 0.2 μm for the 50-0.75 composite membranes. The pore size value was determined when the membrane exhibited 90% of rejection ratio of the PS

nanoparticles with the smallest diameter used. As the effective minimum pore size of the CNF scaffold can be affected by the width of nanofibers and the thickness of the CNF layer, [18] we first evaluated the thickness (or the loading) of the CNF. In Fig. 2e, it was found that when the CNF dry mass was above 0.85 g m^{-2}, the pore size of the cellulose membranes remained around 0.05 µm. While the rejection ratio against PS nanoparticles (0.05 µm) for the 50-0.85 and 50-2.5 membranes increased slightly from 92% to 96%, respectively. However, the extra loading of CNF dramatically reduced the water flux of the membrane (from 134.8 LMH/bar to 4.4 LMH/bar, i.e., about a decrease of 96.8%) because of the low porosity of the CNF layer (< 20%) due to the dense compaction of the CNF scaffold [41, 42]. From this study, the membrane with the CNF loading of 0.85 g m^{-2} appeared to exhibit the optimal filtration performance (i.e., high flux and high rejection ratio). It was interesting to note that the porosity of the cellulose membrane decreased only slightly with the increasing CNF loading (Fig. 2f). All cellulose membranes exhibited high porosity (> 80%) because of the highly porous structure of the Lyocell substrate.

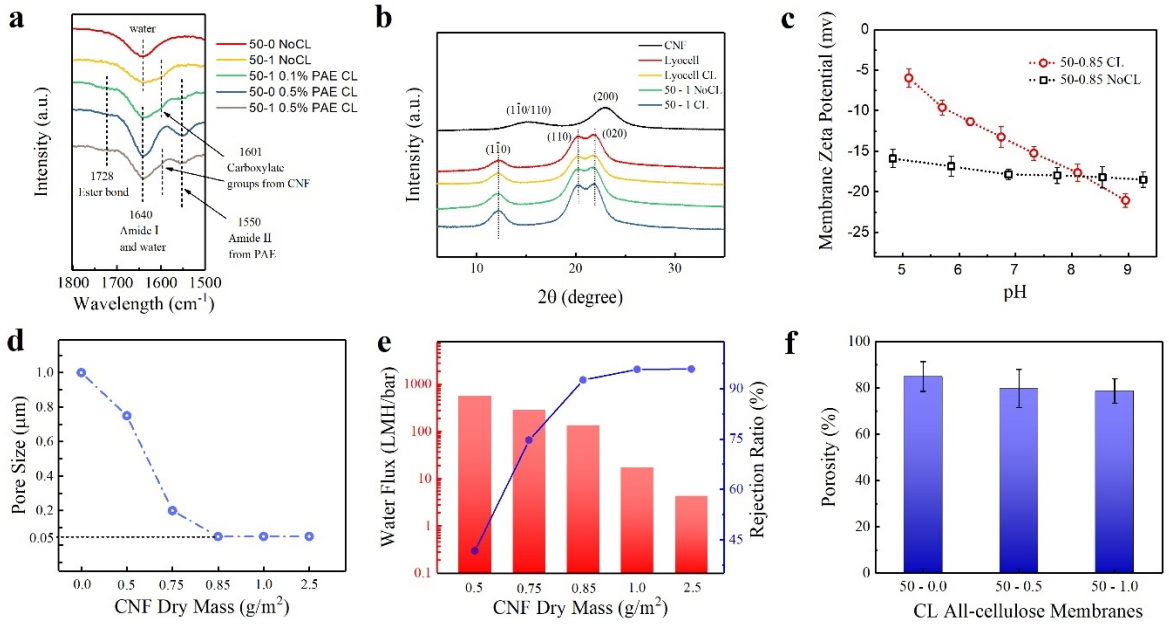

Fig. 2 Characterization of all-cellulose membranes with different CNF loading contents with and without crosslinking. (a) FTIR spectra and (b) XRD patterns of the CNF, lyocell, and cellulose membranes with and without PAE crosslinking (0.1 wt%). (c) Zeta potential analysis of 0.1 wt% PAE crosslinked (CL) and non-crosslinked (No CL) cellulose membranes (50-0.85) as a function of the pH value. (d) Membrane pore size (determined by 90% rejection ratio of PS nanoparticles with the smallest size). (e) Membrane PS solution water flux and 50 nm PS nanoparticles rejection ratio with increasing CNF loading amount (the dry mass of lyocell was 50 g m^{-2}). (f) Porosity of cellulose membranes crosslinked with 0.1 wt% PAE. Data are presented as the mean value (mean ± SD of n=3 repeating tests).

The morphology and nanostructure of cellulose membranes with different CNF loadings (0.0 – 1.0 g m^{-2}) were also characterized by SEM, and the results are illustrated in Fig. 3. The surface images of pure lyocell membrane (crosslinked) showed a highly porous structure defined by the randomly stacked lyocell microfibers with 0.1-0.5 μm diameters (Fig. 3a and 3b). With the addition of 0.85 g m^{-2} CNF, the membrane surface exhibited a smooth cellulose surface without detectable pore structure, even at the micrometer scale (Fig. 3c and 3d). The top view and cross-sectional images of the 50-0.85 crosslinked (CL) membrane (Fig. 3e and 3f, respectively) revealed the hierarchical structure of the membrane comprising a thin CNF layer with a thickness ranging between 50 and 80 nm on top of the microporous lyocell scaffold with an average thickness of 130 ± 25 μm. As the top layer was due to the random agglomeration of CNF, its network formation rendered a pore structure with the size of around 50 nm. This pore size was effective to hinder the passage of uncharged PS nanoparticles with 50 nm diameter, where the PS beads were accumulated on top of the CNF layer due to size exclusion (Fig. 3g and 3h). The intact structure

382 of the CNF layer was also verified by the high rejection ratio (> 92%) against the PS nanoparticles
383 by the cellulose membranes.

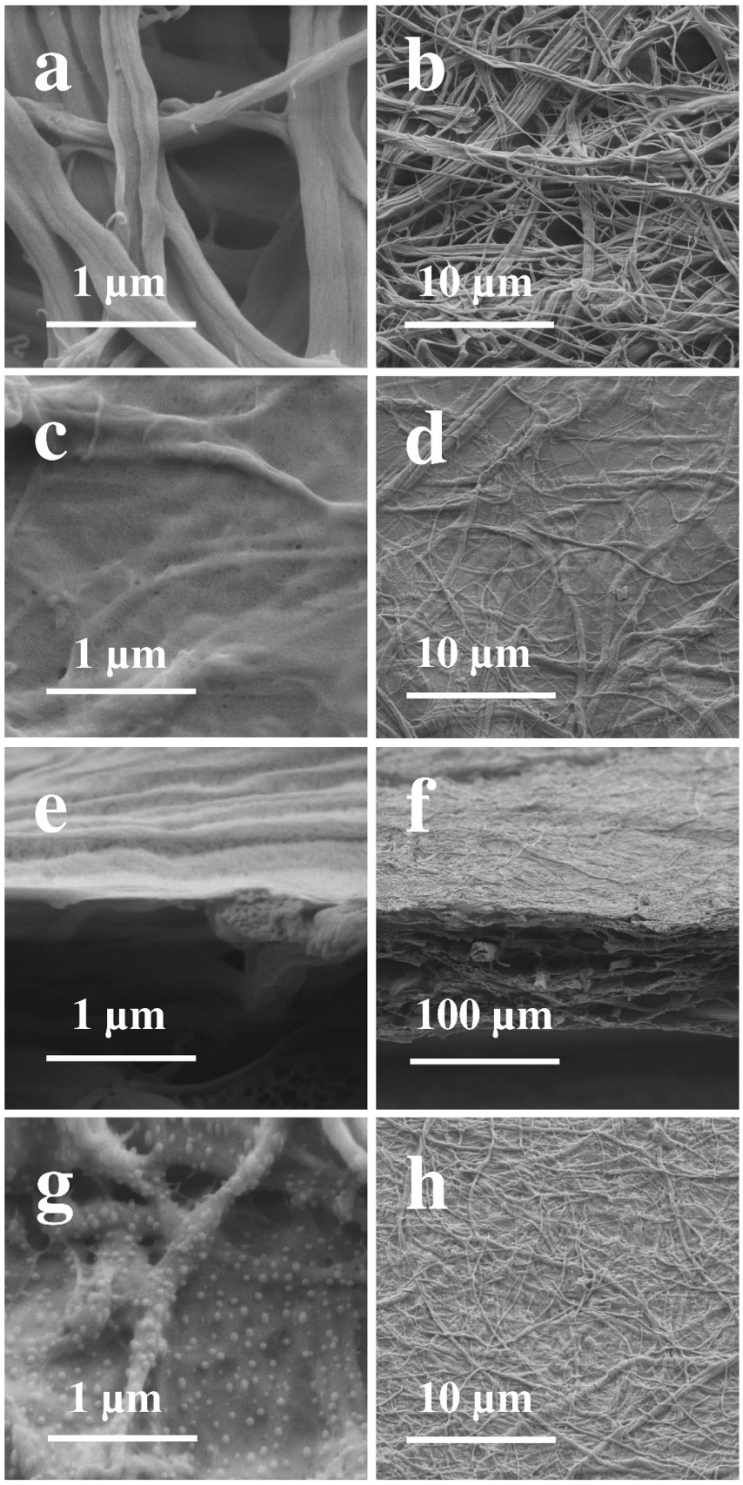

384

Fig. 3 Surface morphology of all-cellulose membrane. (a, b) the 50-0.0 (i.e., pure lyocell) CL membrane, and (c, d) the 50-1.0 (lyocell/CNF) CL membrane; (e, f) cross-sectional morphology of the 50-0.85 CL membrane; (g, h) surface morphology of the 50-0.85 CL membrane after the PS nanoparticles (50 nm) filtration. All the membranes tested were crosslinked with 0.1% PAE.

3.2. Dry and Wet Mechanical Properties of Cellulose Membranes

Tensile testing was performed in both dry and wet states to evaluate the effects of CNF content and PAE crosslinking on the mechanical properties of cellulose membranes. Fig. 4a and 3b illustrate the typical dry and wet stress–strain curves of crosslinked and non-crosslinked cellulose membranes with different CNF loadings, respectively. All dry membranes showed a linear increase up to 3-5 MPa of the tensile stress, followed by a platform and then a continuous stress increment until failure occurred. The plateau in the stress-stress curve showed the plastic flow behavior of cellulose membrane due to the straightening and reorientation of the lyocell fibrous scaffold and interfibrillar slippage [43]. After the reinforcement behavior and following alignment of cellulose fibers, membrane failure occurred because of the failure of fibers and breakage between their existing bonds. The pure lyocell membranes (50-0) exhibited no wet strength before or after crosslinking. Compared with the neat lyocell membrane, the tensile stress of the cellulose membrane increased gradually with the increasing CNF loading. The increasing tensile properties could be attributed to the intra-molecular hydrogen bonding in the CNF network [44]. After chemical crosslinking, the covalent bond formation (ester bonds formed between the

406 azetidinium groups in PAE and carboxyl groups in CNF) in the CNF network inhibited the
407 interfibrillar detachment of the lyocell substrate in both dry and wet conditions.

408

409 It was noted that the crosslinking reaction slightly decreased the strength of the cellulose
410 membrane but greatly enhanced the membrane toughness, especially in the wet state (Fig. 4c and
411 4d). For example, the wet strength of the 50-1 cellulose membrane increased by 190 % after the
412 PAE crosslinking (from 2.8 ± 0.3 MPa to 8.1 ± 0.5 MPa), while the wet toughness of the
413 crosslinked 50-1 membrane (0.78 MPa) became twice of the non-crosslinked 50-1 membrane (0.36
414 MPa). These results are consistent with the observations made in a previous study that the wet
415 strength of cellulose paper was found to increase when both PAE and CNF were absorbed onto
416 cellulose fibers [45].

417

418 The wet mechanical properties (i.e., the maximum stress in the stress-strain curve) of wet
419 cellulose membranes and other reported membranes under the similar wet conditions [46-51] are
420 illustrated in Fig. 4e, while the maximum stress change of the crosslinked 50-0.85 (CL 50-0.85)
421 membrane at varying water immersion time (up to 14 days) is shown in Fig. 4f. In Fig. 4e, it was
422 seen that composite membranes without the incorporation of enhancing additives or
423 physical/chemical crosslinking usually exhibited low mechanical properties. However, the
424 cellulose membrane (CL 50-1.0) with a high loading of CNF crosslinked by PAE showed
425 competitive maximum wet stress or wet strength in comparison with those from published
426 composite membranes, confirming the potential of cellulose membranes for practical applications.
427 In Fig. 4e, the wet strength of the cellulose membrane (CL 50-0.85) was found to decrease by

about 20% after 7-day immersion probably because of the water-swollen effect, however this property remained unchanged at 3.8 ± 0.6 MPa for the rest of the test.

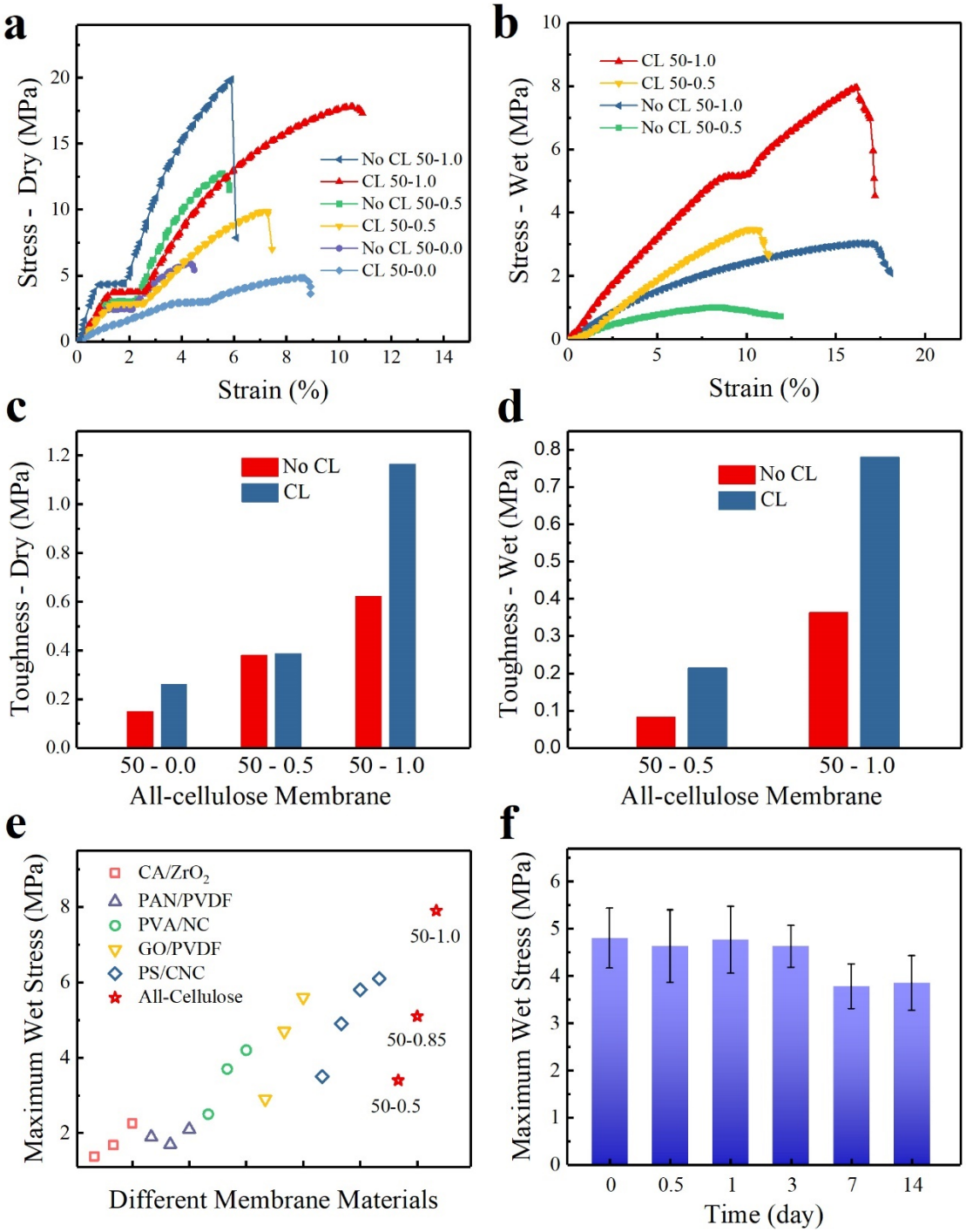

Fig. 4 Mechanical performance of all-cellulose membranes. Stress–strain curves and calculated toughness of (a, c) dry and (b, d) wet cellulose membranes with and without crosslinking (0.1 wt % PAE). (e) Comparison of the maximum wet stress values of cellulose membranes (crosslinked with 0.1 wt % PAE) with those of other reported membranes. Symbols indicate the data points of reported membranes with different composite ratio. (f) The maximum wet stress change from a 14-day wet immersion test of the CL 50-0.85 membrane. Bars represent the mean values ± SD based on three independent tests.

3.3. Wastewater/MLSS Ultrafiltration Performance of Cellulose Membranes

The dynamic UF test was performed to evaluate the filtration performance and fouling behavior of cellulose membranes using MLSS with an original turbidity of 537 ± 98 nephelometric turbidity unit (NTU) and total dissolved solids (TDS) of 890 ± 102 mg L^{-1}. In this study, commercial UF membranes (PVDF-V6, PVDF-A6, and PES-LX) with a similar pore size range and initial water flux (as those of cellulose membranes) were also selected to provide the benchmark values for comparison. The general properties of cellulose and selected polymeric UF membranes are summarized in Table S2 (*Supporting Information*). The results the dynamic UF test are illustrated in Fig. 5. In Fig. 5a, it was found that all membranes experienced a water flux decline over the filtration operation because of the fouling issue. However, the PVDF-A6 membrane displayed a steeper decrease than cellulose and PVDF-V6 membranes because of the hydrophobic nature of the PVDF-A6 membrane, resulting in a greater fouling tendency and flux decay. In contrast, the PES-LX membrane suffered the smallest flux decrease but it exhibited the

lowest initial permeation flux. It was seen that the permeation flux of cellulose and PVDF-V6 membranes could be near fully recovered after hydraulic washing and NaClO cleaning, while hydrophobic membranes (PVDF-A6 and PES-LX) suffered irreversible fouling resulting poor flux recovery (below 23 LMH) after the first run. In this study, the turbidity of all tested permeates was below 0.3 NTU (a photograph of wastewater and filtrated permeate is shown in Fig. 5b), which met the target requirement of 0.3 NTU for public water systems recommended by the United States Environmental Protection Agency (USEPA) [52]. It is noteworthy to point out that, the permeate TDS by using the cellulose membrane was less than 400 ppm, lower than those of polymeric membranes (Fig. 5c). Although the rejection ratio of all tested membranes was above 99.9%, the recovery of permeation flux for these membranes using NaClO cleaning was slightly higher than that using hydraulic washing (Fig. 5d). The usage of NaClO to remove organic and microbial foulants, commonly absorbed on the membrane surface, is a well adopted approach to cleanse the used membrane in wastewater treatment [53, 54]. Among all tested membranes, the cellulose membrane (CL 50-0.85) exhibited the highest flux recovery ratio (88 ± 4.5 % for hydraulic wash and 97 ±1.5 % for NaClO cleaning). This indicates that the fouling layer developed on the cellulose membrane surface, which contains abundant hydrophilic hydroxyl and carboxyl groups, is easier to remove than those on the polymeric membrane surfaces either by water or NaClO cleaning.

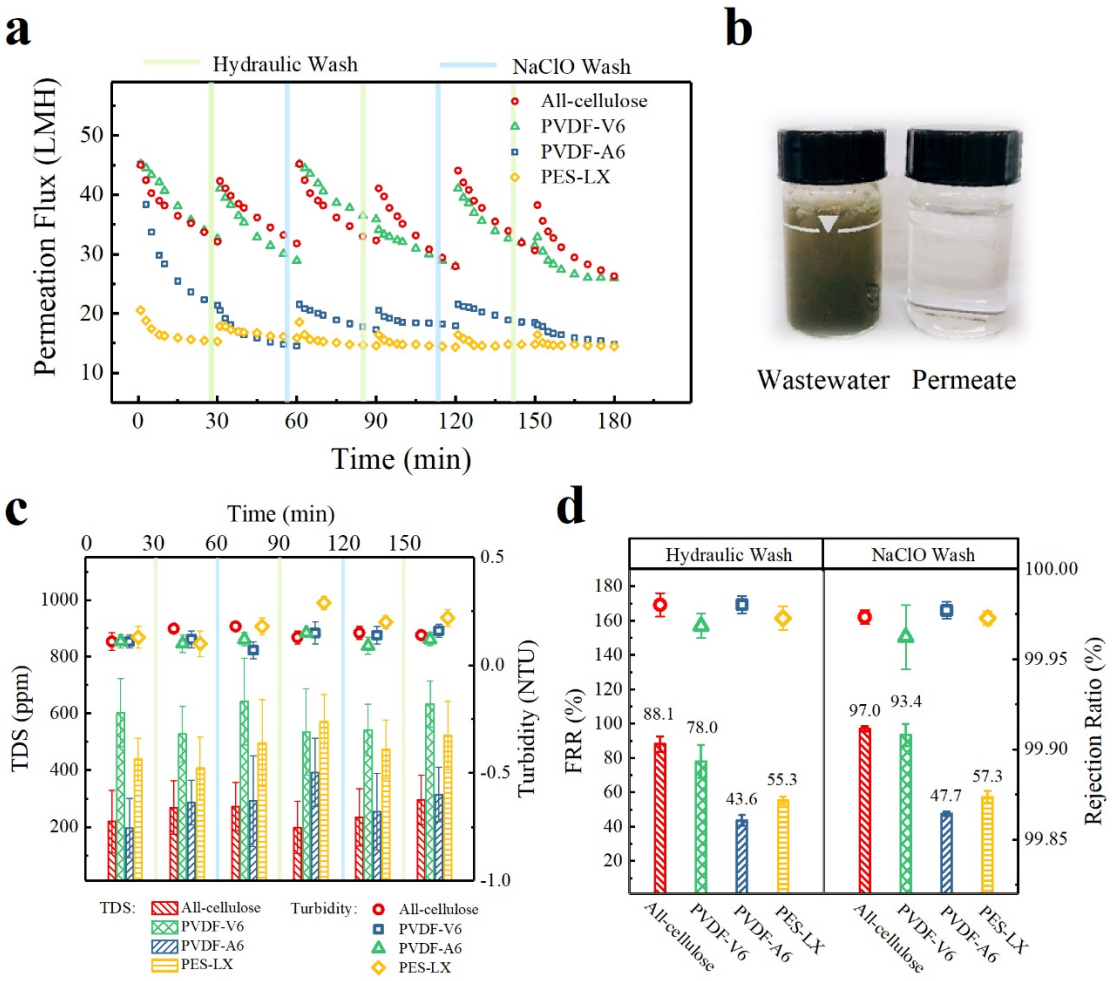

Fig. 5 Wastewater filtration performance of all-cellulose and commercial membranes. (a) Filtration cycles with multiple permeation flux recoveries for cellulose (CL 50-0.85), PVDF-V6 (modified PVDF), PVDF-A6, and PES-LX membranes using alternative hydraulic wash and NaClO wash. (b) Photograph of original wastewater and filtrated permeate. (c) Total dissolved solid (TDS - columns) and turbidity (symbols) changes in wastewater filtration. (d) Water flux recovery ratio and rejection ratio of cellulose (CL 50-0.85), PVDF-V6, PVDF-A6, and PES-LX membranes after hydraulic and NaClO cleaning. Data are presented as mean ± SD of n=3 repeats.

3.4. Wastewater Fouling Mechanism Study

Soluble microbial products (SMP) and extracellular polymeric substances (EPS, the products of substrate metabolism and biomass decay) are major contributors to the membrane fouling problem in MBRs. These foulants consist of humic substances, proteins, lipids, polysaccharides, carbohydrates and macromolecules [55, 56]. Fig. 6a illustrates the surface characteristics, determined by IR spectra, of pristine, fouled, and cleaned cellulose (CL 50-0.85) of polymeric membranes. The characteristic peaks of the foulants occurred mainly in the wavelength range of 1500-1800 cm^{-1} and 3100-3400 cm^{-1}. Compared with the FTIR spectra of pristine membranes, the fouled membranes exhibited four new peaks at 1542 cm^{-1} (C=N vibration of amide II), 1651 cm^{-1} (C=O vibration of amide I and humics), 1731 cm^{-1} (C=O vibration in protein), and 3282 cm^{-1} (N-H stretching in protein and humic substance), which were in accordance with the characteristic peaks of protein and humic foulants [57, 58]. These results confirmed that membrane fouling was mainly caused by the C=O and C=N amide groups in protein molecules and the N-H groups in polysaccharides. It was seen that the cellulose membrane suffered a less tendency fouling, as revealed by the similar spectra from the pristine and fouled cellulose membranes. After NaClO cleaning, the difference in the spectra between all the pristine and cleaned cellulose membranes was negligible, indicating the high efficiency of NaClO in removing the organic and microbial foulants deposited on the cellulose surface [59].

Although the removal of the cake layer on the membrane surface can elute a large proportion of the foulants, a small fraction of foulants could still remain inside the membrane pores

503 and cause irreversible fouling. However, this is not clear by the FTIR results. To understand the
504 detailed fouling process, other characterizations of the fouled and cleaned membranes were also
505 carried out, including the contact angle measurement to determine the hydrophilicity and zeta
506 potential measurements to determine the membrane surface charge, where the results from
507 membranes being fouled by wastewater and being treated by NaClO cleaning are shown in Fig. 6b
508 and 6c. In Fig. 6b, the contact angle (CA) of the pristine cellulose membrane (~ 0º) indicated that
509 its surface was truly hydrophilic, whereas the polymeric membranes were relatively hydrophobic
510 with higher CA values (50º - 70º). In comparison with the pristine membranes, the CA values of
511 all fouled membranes became more hydrophobic due to the deposition of hydrophobic foulants on
512 the membrane surface [60]. After NaClO cleaning, only cellulose and PVDF-V6 membranes
513 exhibited CA values close to their initial values. The CA value of the cleaned PVDF-A6 and PES
514 membranes was somewhat higher than that of the membranes because of the presence of residual
515 hydrophobic foulants on the membrane surface, even after the cleaning treatment [61]. The CA
516 results agreed with the results observed in the flux recovery test that polymeric membranes
517 suffered more irreversible fouling during wastewater filtration (Fig. 5a).

518

519 The zeta potential test was also carried out to characterize the fouling behavior of the
520 membranes, where the results could be used to optimize the membrane cleaning efficiency [62].
521 In Fig. 6b, the pristine cellulose (CL 50-0.85), PVDF-A6, PES-LX membranes typically exhibited
522 negative zeta potential values. As the PVDF-V6 membrane contained modified-PVDF (described
523 by the manufacturer) possibly with the amine groups (as seen by the N-H peak at 1560 cm^{-1} in the
524 FTIR spectrum, Fig. 6a), this membrane exhibited a positive zeta potential value at neutral pH [63].
525 The negative zeta potential of the fouled PVDF-V6 membranes indicated the deposition of foulants

such as biomacromolecules and hydrophobic organic matter in wastewater are all negatively charged, which has been reported previously [64, 65]. It was interesting to note that the pristine, fouled and cleaned cellulose membranes exhibited similar negative zeta potential values (Fig. 6b), which implied that only minor fouling occurred on the cellulose membrane surface. This could be explained by the weak interactions between the foulants and nanocellulose, as the charge repulsion would hinder the already weak hydrophobic aggregation, resulting in less adhesion/adsorption of biomolecular contaminants on the cellulose membrane surface [18]. Although electrostatic repulsion might also exist between the foulants and negatively charged PVDF-A6 and PES-LX membranes, the stronger hydrophobic-hydrophobic interactions would dominate the fouling process. Meanwhile, the zeta potential of all NaClO cleaned polymeric membranes was altered probably due to the occurrence of the reaction between the polymeric scaffold and NaClO [54, 66].

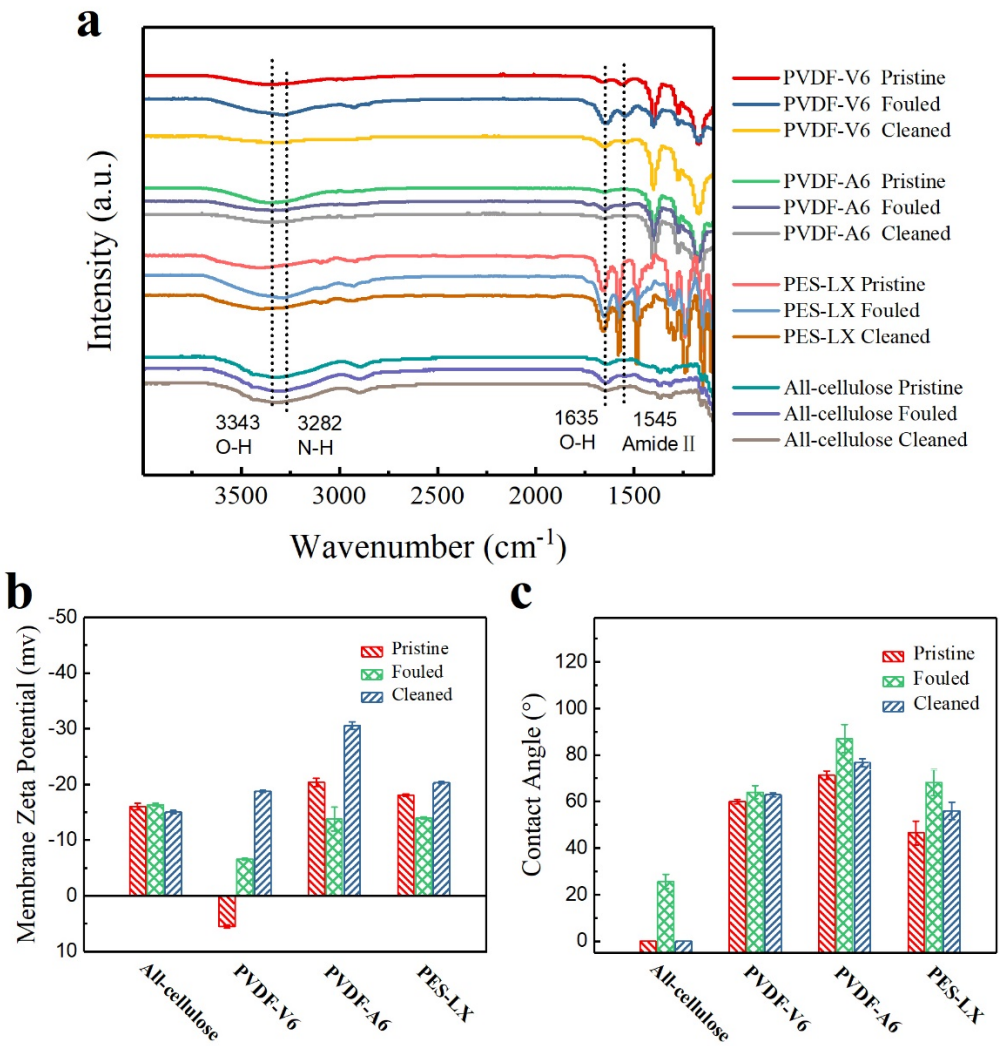

537

538 **Fig. 6** Characterization of membrane before and after the wastewater filtration. (a) FT-IR

539 spectra, (b) membrane zeta potential (pH = 7; 1 mM KCl), and (c) water contact angle of the

540 pristine, wastewater fouled, and NaClO cleaned membranes (the chosen cellulose membrane was

541 CL 50-0.85). Bars are presented as mean ± SD of n=3 individual tests.

542

543

544 The fouling resistances parameters, such as total membrane resistance (R_t), intrinsic
545 resistance (R_m) and fouling resistance (R_f) were characterized using the resistance-in-series model
546 to reveal the mechanism of membrane fouling [27]. As illustrated in Fig. 7a, the cellulose
547 membrane and modified PVDF membrane (PVDF-V6) exhibited lower R_t and R_f, while the
548 conventional PVDF-A6 and PES membranes showed more severe total fouling. Detailed analysis
549 in Fig. 7b indicated that cellulose and modified PVDF membranes possessed a high reversible
550 fouling percentage (R_c/R_f) and a low irreversible fouling percentage (R_p/R_f). This implied that the
551 removable cake layer fouling dominated the total fouling during wastewater filtration. The results
552 can also be specified by their high flux recovery ratio after NaClO or hydraulic cleaning (Fig. 5d).
553 Based on the contact angle and zeta potential results, the low R_t and R_p/R_c values of cellulose
554 membrane could be attributed to the integration of negatively charged and hydrophilic CNF, which
555 has been shown to decrease the irreversible fouling and increase the antifouling property of
556 membranes [18]. On the other hand, the low fouling tendency of modified PVDF membrane could
557 be attributed to the usage of zwitterionic polymer, as indicated by the FTIR and zeta potential
558 results from the PVDF-A6 membrane (Fig. 6a and 6b) [67].

559

560 To further understand the fouling mechanism during wastewater filtration, the
561 accumulative permeate volume versus time data of cellulose (CL 50-0.85), PVDF (V6 and A6),
562 and PES membranes was fitted with three combined models: cake filtration-complete blockage
563 model (CFCBM), cake filtration-intermediate blockage model (CFIBM) and cake filtration-
564 standard blockage model (CFSBM). The best fit was determined by comparing the difference
565 between the data points and model's prediction values, when the smallest sum of squared residuals
566 (SSR) value was reached [27, 31]. As demonstrated in Fig. 7c, 7f and Table S3 (*Supporting*

Information), the combined CFCBM was in good agreement with the experimental data for all tested membranes, regarding the lowest SSR and highest R^2 values. While the membrane encountered total resistance from both cake layer and complete pore blocking, the CFCBM model specified that the formation of foulant cake layer and complete membrane blocking could occur simultaneously rather than independently, as suggested by the single fouling model. While the rate of foulant precipitation on the membrane surface depended on the adjacent pore blockage, the rate of complete blocking was lower due to the resistance of foulant formation as a cake layer. Moreover, we speculate that the rapid flux decay (in a single filtration run) was mainly caused by cake layer fouling mechanism instead of the complete blocking mechanism because of the lower K_b value compared to K_c for all tested membranes [31, 68].

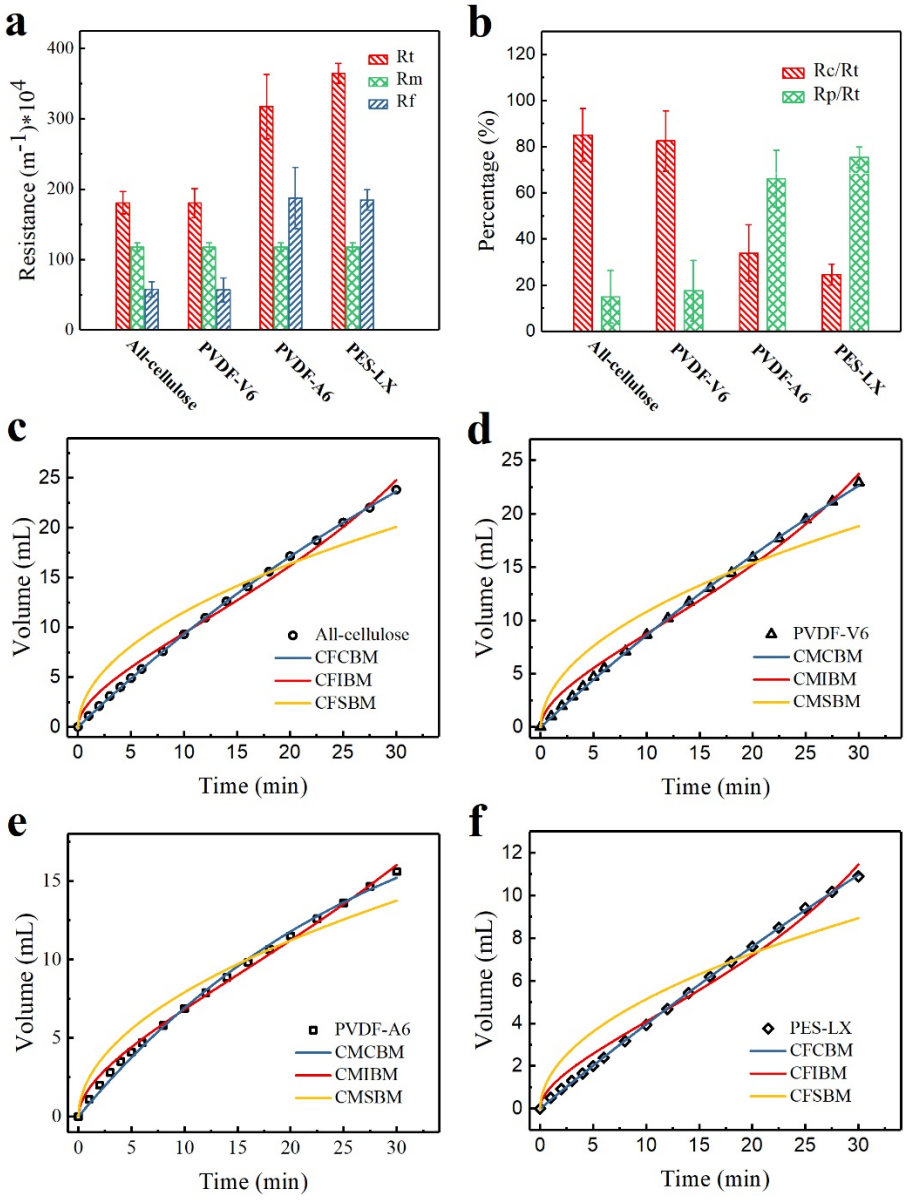

577

578 **Fig. 7** Mechanism study of membrane fouling by calculating the fouling resistances parameters
579 and fitting with CFCBM, CFIBM, and CFSBM models. (a) Summary of the total resistance (R_t),
580 inherent membrane resistance (R_M) and fouling resistance (R_f), (b) reversible fouling ratio
581 (R_C/R_f) and irreversible fouling ratio (R_P/R_f) of cellulose and polymeric membranes during the
582 flux recovery experiment of wastewater filtration. (c-f) Experimental and predictive permeation
583 volume as a function of filtration time among different combined models of cellulose (CL 50-

584 0.85), PVDF-V6, PVDF-A6, and PES-LX membranes. Bars are presented as mean ± SD of n=3
585 individual tests.

586

587 **3.5. Reproducibility and Durability of Cellulose Membranes**

588

589 The unique features of the demonstrated cellulose membranes include good reproducibility
590 and durability for the successful ultrafiltration process. For example, the normalized permeation
591 flux (J_w/J_o) at the initial water flux (46.0 LMH) during 16 consecutive wastewater filtration runs
592 was monitored (Fig. 8a) to illustrate the reproducibility of the representative cellulose membrane
593 (CL 50-0.85). This membrane exhibited excellent flux recovery and easy to clean properties (e.g.,
594 using 30-second NaClO cleaning), as indicated by the high flux recovery ratio (> 95%) and high
595 turbidity rejection ratio (> 99.95%) during the 16-cycle test run (Fig. 8b).

596

597 Furthermore, a 12-hour continuous wastewater filtration test was conducted to demonstrate
598 the long-time stability of this cellulose membrane using an immersed membrane filtration system
599 (schematically shown in Fig. S2, *Supporting Information*), which was commonly adopted in
600 industrial membrane bioreactor. As the flux-time data displayed in Fig. 8c, the permeate flux
601 declined from the initial value of 58.3 LMH to 37.2 LMH in the first two hours because of the
602 simultaneous occurrence of cake layer fouling and pore blocking fouling. After 12-hour filtration
603 under a constant pressure (0.5 bar), both high permeate flux (33 LMH) and good rejection ratio
604 (>99.95%) were maintained. These results indicated good stability and durability of the

demonstrated cellulose membrane and its excellent filtration efficiency under a lengthy operation cycle.

To evaluate this membrane for practical applications, the durability of the cellulose membrane (CL 50-0.85) was further evaluated at two different pH values (2.5 and 9.0) and elevated temperature (60 ºC) [69]. As illustrated in Fig. 8d, the permeation flux of the cellulose membranes treated with acid and warm water was similar to the original membrane. As for the membrane immersed in a pH = 9.0 buffer, the permeation flux increased slightly because the cellulose component could degrade slowly under alkaline conditions [70]. Regardless of the different treatment, the turbidity of all permeates maintained a low value (< 0.3 NTU), indicating that the cellulose membrane was relatively stable for use over a wide pH and temperature range.

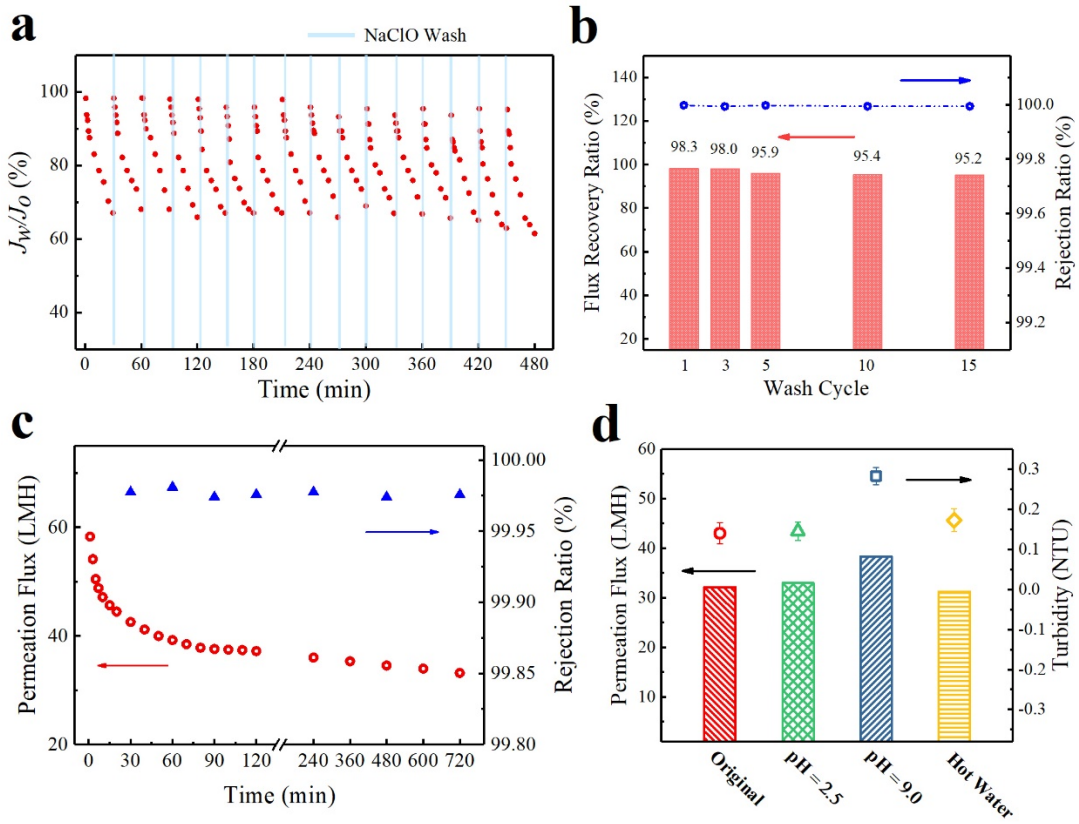

Fig. 8 Reproducibility and durability test of cellulose membrane. (a) Ratio of permeation water flux (J_w) over initial water flux (J_o), (b) flux recovery ratio and turbidity rejection ratio over 16-cycle wastewater runs of CL 50-0.85 membrane. (c) Long term wastewater filtration of CL 50-0.85 membrane using the immersed membrane filtration system and the corresponding rejection ratio in terms of the turbidity. (d) Durability test of the CL 50-0.85 membrane evaluated regarding two critical pH values (immersed in pH = 2.5 and 9.0 buffer solutions for three days) and temperature (immersed in 60 ºC warm water for 7 days) resistance. Bars presented the permeation flux data, and the symbols presented the turbidity data (mean ± SD of n=3 independent tests).

In the scratch test, the permeability of cellulose (CL 50-0.85) and polymeric membranes was evaluated prior to and immediately after the damage. After around 10-µm wide blade scratch was applied, the permeability of the cellulose membrane instantly increased to 135 ± 5 % and then returned to 102 ± 3 % of the starting permeability after a 10-minute distilled water run. On the other hand, the permeability of polymeric membranes surged after the scratch and could not drop back to the original values within the testing time (Fig. 9a). Furthermore, the wastewater filtration test of the scratched cellulose membrane exhibited the same trend observed in the distilled water run (Fig. 9a and 9b). It was seen that after scratching, the permeate flux and turbidity of the cellulose membrane increased immediately and then gradually returned to the starting value in about 20 minutes during filtration. The SEM image of the healed scratch on the used cellulose membrane verified its self-healing ability (Fig. 9c). The results indicated that cellulose nanofibers were able to form a new layer to cover the damage on the membrane surface. Similar studies indicating the self-healing ability of CNF-based hydrogels, such as the chitosan/CNF system or

nanocomposite/polymer system, have been reported previously [71]. The self-healing ability of the CNF layer can be explained as follows. When the scratch is form, the high mobility of CNFs will allow them to migrate towards the damage area and minimize the increased surface tension. Upon contact, CNFs will aggregate in the wet state due to strong hydrophobic interactions forming a new layer to hear the damage. The layer can be further stabilized by the formation of hydrogen bonds between the abundant hydroxyl groups and carboxyl groups on CNFs [72]. Aside for the above feature, cellulose membrane exhibited another unique feature, that is the superior flexibility and ductility over polymeric membranes, which is seen in Fig. 9d. When immersed in water, the twisted (deformed) cellulose membrane could quickly recover back to its original shape without cracks or deformation. This ensures the practical usage of cellulose membranes when the membrane needs to be warped, folded, or twisted during manufacturing or handling.

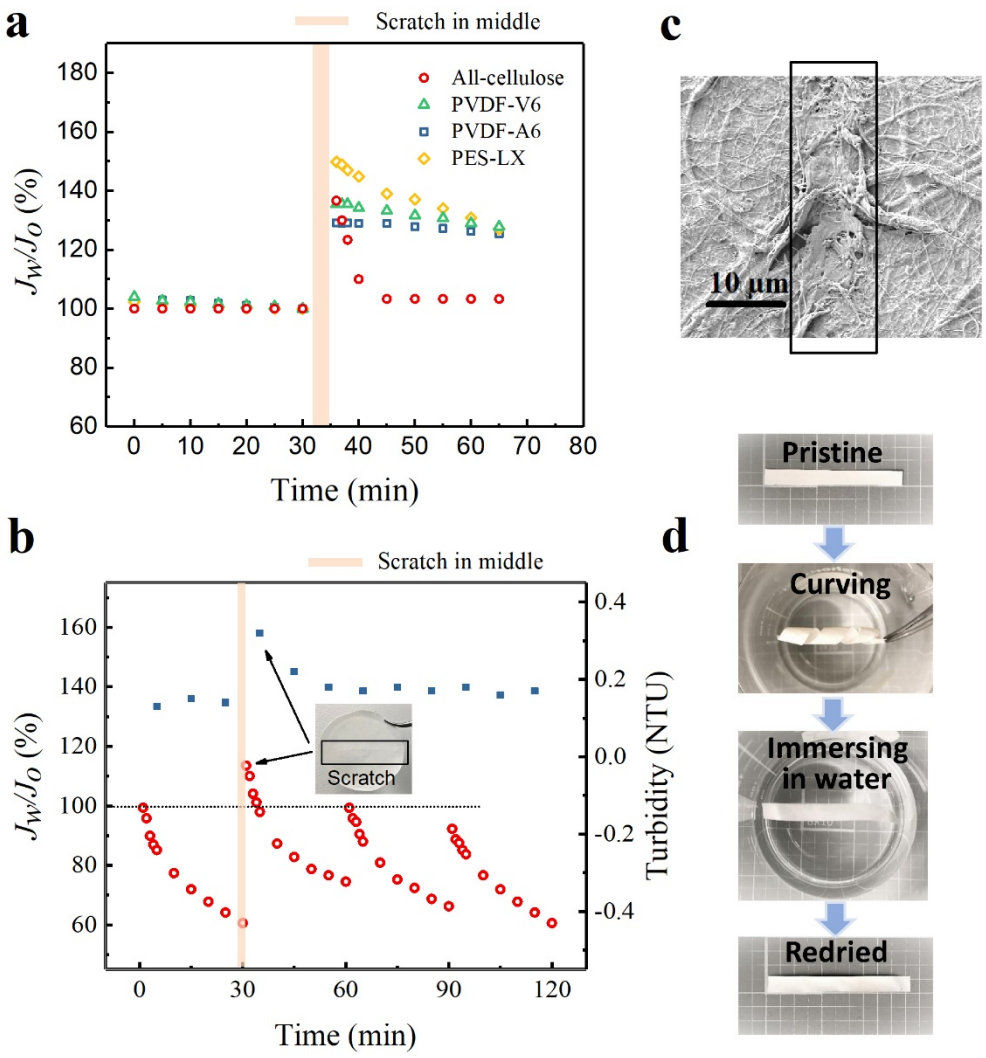

651

652 **Fig. 9** Self-healing property of all-cellulose membrane. The self-healing performance was
653 indicated by how soon the membrane water flux can return to the original level after scratching
654 membrane for 3cm in the middle using a 10-μm wide blade. (a) Scratch test of cellulose (CL 50-
655 0.85) and polymeric membranes regarding the distilled water filtration. (b) Scratch test of
656 cellulose (CL 50-0.85) regarding the wastewater filtration performance and permeate turbidity
657 during cyclic operation with hydraulic cleaning. (c) SEM image of the self-healed cellulose
658 membrane after the scratch test of distilled water filtration. (d) Shape recovery test of the

cellulose membrane by curving and subsequent water immersion. Result presented the mean value of n=3 independent repeats.

4. Conclusions

A robust and nanostructured cellulose membrane system with high porosity (~ 80%) was prepared by incorporating CNF into a lyocell microfibrous scaffold following by a crosslinking reaction among nanofibers. In the multiple-run wastewater filtration test, the optimized cellulose membrane exhibited high permeation flux (127.6 ± 21.8 L m^{-2} h^{-1} bar^{-1}), excellent separation efficiency (> 99.9%), good flux recovery ratio (> 95%) and self-healing ability. Compared with commercial polymeric membranes, such as PVDF and PES membranes, the cellulose membrane showed superior filtration performance after NaClO and pure hydraulic cleaning as demonstrated by the FTIR, contact angle, and zeta potential characterizations. The polymer membranes suffered severe irreversible fouling during wastewater filtration. However, the reversible fouling seemed to dominate the total fouling of cellulose membrane and was revealed by the fouling mechanism study using the resistance-in-series model and three combined cake-filtration models. In addition, the cellulose membranes showed excellent flexibility, pH resistance, stability in hot water, and durability with good mechanical strength (the wet strength was 3.5 - 8.0 MPa). The easy to clean characteristics of the cellulose membrane could be attributed to the negative charges and hydrophilic membrane surface because of the presence of CNF. The sustainability, low cost, good mechanical strength, and filtration performance of cellulose membranes make them promising alternative for polymeric ultrafiltration membranes in wastewater treatments.

CRediT Authorship Contribution Statement

Mengying Yang: Conceptualization, Methodology, Data curation, Writing - original draft, Sarah Lotfikatouli: Methodology, Review & editing. Yvonne Chen: Methodology, Visualization, Validation. Tony Li: Methodology, Validation. Hongyang Ma: Writing - review & editing, Validation. Xinwei Mao: Writing - review & editing, Validation. Benjamin S. Hsiao: Funding acquisition, Writing - review & editing, Supervision, Validation.

Acknowledgement

We acknowledge the financial support from the Polymer Program of the Division of Materials Research in the National Science Foundation (DMR-1808690). The authors would also like to thank the Advanced Energy Research and Technology Center (AERTC) and Central Microscopy Imaging Center (CMIC) at the Stony Brook University for the SEM and TEM measurements.

Reference

[1] A. Gallego-Schmid, R.R.Z. Tarpani, Life cycle assessment of wastewater treatment in developing countries: A review, Water Res, 153 (2019) 63-79.

[2] L. Petta, S. De Gisi, P. Casella, R. Farina, M. Notarnicola, Evaluation of the treatability of a winery distillery (vinasse) wastewater by UASB, anoxic-aerobic UF-MBR and chemical precipitation/adsorption, J Environ Manage, 201 (2017) 177-189.

[3] H. Maleki, N. Husing, Current status, opportunities and challenges in catalytic and photocatalytic applications of aerogels: Environmental protection aspects, Appl Catal B-Environ, 221 (2018) 530-555.

[4] C. Shen, Y.Q. Zhao, W.X. Li, Y. Yang, R.B. Liu, D. Morgen, Global profile of heavy metals and semimetals adsorption using drinking water treatment residual, Chem Eng J, 372 (2019) 1019-1027.

[5] E.O. Ezugbe, S. Rathilal, Membrane Technologies in Wastewater Treatment: A Review, Membranes-Basel, 10 (2020).

[6] N.H. Ismail, W.N.W. Salleh, A.F. Ismail, H. Hasbullah, N. Yusof, F. Aziz, J. Jaafar, Hydrophilic polymer-based membrane for oily wastewater treatment: A review, Sep Purif Technol, 233 (2020).

[7] C.H. Koo, A.W. Mohammad, F. Suja', M.Z.M. Talib, Review of the effect of selected physicochemical factors on membrane fouling propensity based on fouling indices, Desalination, 287 (2012) 167-177.

[8] P. Krzeminski, L. Leverette, S. Malamis, E. Katsou, Membrane bioreactors - A review on recent developments in energy reduction, fouling control, novel configurations, LCA and market prospects, J Membrane Sci, 527 (2017) 207-227.

[9] C. Stone, F.M. Windsor, M. Munday, I. Durance, Natural or synthetic - how global trends in textile usage threaten freshwater environments, Sci Total Environ, 718 (2020).

[10] Y.H. Xu, Q. He, C.H. Liu, X.L. Huangfu, Are Micro- or Nanoplastics Leached from Drinking Water Distribution Systems?, Environ Sci Technol, 53 (2019) 9339-9340.

[11] M. Jonoobi, R. Oladi, Y. Davoudpour, K. Oksman, A. Dufresne, Y. Hamzeh, R. Davoodi, Different preparation methods and properties of nanostructured cellulose from various natural resources and residues: a review, Cellulose, 22 (2015) 935-969.

[12] Y. Huang, P. Yang, F. Yang, C. Chang, Self-supported nanoporous lysozyme/nanocellulose membranes for multifunctional wastewater purification, J Membrane Sci, 635 (2021).

[13] K. Peng, Y. Huang, N. Peng, C. Chang, Antibacterial nanocellulose membranes coated with silver nanoparticles for oil/water emulsions separation, Carbohydr Polym, 278 (2022) 118929.

[14] N. Mohammed, N. Grishkewich, K.C. Tam, Cellulose nanomaterials: promising sustainable nanomaterials for application in water/wastewater treatment processes, Environ Sci-Nano, 5 (2018) 623-658.

[15] R.E. Abouzeid, R. Khiari, N. El-Wakil, A. Dufresne, Current State and New Trends in the Use of Cellulose Nanomaterials for Wastewater Treatment, Biomacromolecules, 20 (2019) 573-597.

[16] K. Oksman, Y. Aitomaki, A.P. Mathew, G. Siqueira, Q. Zhou, S. Butylina, S. Tanpichai, X.J. Zhou, S. Hooshmand, Review of the recent developments in cellulose nanocomposite processing, Compos Part a-Appl S, 83 (2016) 2-18.

[17] P. Hadi, M.Y. Yang, H.Y. Ma, X.Y. Huang, H. Walker, B.S. Hsiao, Biofouling-resistant nanocellulose layer in hierarchical polymeric membranes: Synthesis, characterization and performance, J Membrane Sci, 579 (2019) 162-171.

[18] M.H. Yang, P. Yin, X. Yu, J. Huang, X. Ma, H. Walker, H. Hsiao, B.S., Antifouling nanocellulose membranes: How subtle adjustment of surface charge lead to self-cleaning property, J Membrane Sci, 618 (2021) 118739.

747 [19] S. Lotfikatouli, P. Hadi, M. Yang, H.W. Walker, B.S. Hsiao, C. Gobler, X. Mao, Enhanced
748 anti-fouling performance in Membrane Bioreactors using a novel cellulose nanofiber-coated
749 membrane, Sep Purif Technol, 275 (2021) 119145.
750 [20] D. Li, X.Y. Huang, Y.N. Huang, J. Yuan, D. Huang, G.J. Cheng, L.N. Zhang, C.Y. Chang,
751 Additive Printed All-Cellulose Membranes with Hierarchical Structure for Highly Efficient
752 Separation of Oil/Water Nanoemulsions, Acs Appl Mater Inter, 11 (2019) 44375-44382.
753 [21] C.H. Ao, J.Q. Zhao, Q.Y. Li, J. Zhang, B.X. Huang, Q.H. Wang, J.G. Gai, Z.M. Chen, W.
754 Zhang, C.H. Lu, Biodegradable all-cellulose composite membranes for simultaneous oil/water
755 separation and dye removal from water, Carbohyd Polym, 250 (2020).
756 [22] N.A. Awang, W.N.W. Salleh, A.F. Ismail, N. Yusof, F. Aziz, J. Jaafar, Adsorption Behavior
757 of Chromium(VI) onto Regenerated Cellulose Membrane, Ind Eng Chem Res, 58 (2019) 720-
758 728.
759 [23] L.A. Goetz, N. Naseri, S.S. Nair, Z. Karim, A.P. Mathew, All cellulose electrospun water
760 purification membranes nanotextured using cellulose nanocrystals, Cellulose, 25 (2018) 3011-
761 3023.
762 [24] L.L. Kong, D.L. Zhang, Z.Q. Shao, B.X. Han, Y.X. Lv, K.Z. Gao, X.Q. Peng, Superior effect
763 of TEMPO-oxidized cellulose nanofibrils (TOCNs) on the performance of cellulose triacetate
764 (CTA) ultrafiltration membrane, Desalination, 332 (2014) 117-125.
765 [25] A. Isogai, T. Saito, H. Fukuzumi, TEMPO-oxidized cellulose nanofibers, Nanoscale, 3 (2011)
766 71-85.
767 [26] L.P. Thomas, B.M. Marino, R.N. Szupiany, M.N. Gallo, Characterisation of the suspended
768 particulate matter in a stratified estuarine environment employing complementary techniques,
769 Cont Shelf Res, 148 (2017) 37-43.

770 [27] J.L. Lv, G.Q. Zhang, H.M. Zhang, F.L. Yang, Graphene oxide-cellulose nanocrystal (GO-
771 CNC) composite functionalized PVDF membrane with improved antifouling performance in
772 MBR: Behavior and mechanism, Chem Eng J, 352 (2018) 765-773.
773 [28] S.L.D. Kenari, B. Barbeau, Understanding ultrafiltration fouling of ceramic and polymeric
774 membranes caused by oxidized iron and manganese in water treatment, J Membrane Sci, 516
775 (2016) 1-12.
776 [29] M. Sampath, A. Shukla, A.S. Rathore, Modeling of Filtration Processes-Microfiltration and
777 Depth Filtration for Harvest of a Therapeutic Protein Expressed in Pichia pastoris at Constant
778 Pressure, Bioengineering (Basel), 1 (2014) 260-277.
779 [30] S.R. Sowmya, G.M. Madhu, A. Raizada, C.D. Madhusoodana, Studies on effective treatment
780 of waste water using submerged ceramic membrane bioreactor, Mater Today-Proc, 24 (2020)
781 1251-1262.
782 [31] G. Bolton, D. LaCasse, R. Kuriyel, Combined models of membrane fouling: Development
783 and application to microfiltration and ultrafiltration of biological fluids, J Membrane Sci, 277
784 (2006) 75-84.
785 [32] P.R. Naegeli, J.T. Clerc, Computer System for Structural Identification of Organic
786 Compounds from Spectroscopic Data, Anal Chem, 46 (1974) A739-A744.
787 [33] T. Obokata, A. Isogai, The mechanism of wet-strength development of cellulose sheets
788 prepared with polyamideamine-epichlorohydrin (PAE) resin, Colloid Surface A, 302 (2007)
789 525-531.
790 [34] W.S. Yang, H.Y. Bian, L. Jiao, W.B. Wu, Y.L. Deng, H.Q. Dai, High wet-strength, thermally
791 stable and transparent TEMPO-oxidized cellulose nanofibril film via cross-linking with poly-
792 amide epichlorohydrin resin, Rsc Adv, 7 (2017) 31567-31573.

[35] W. Zhang, Y. Zhang, C.H. Lu, Y.L. Deng, Aerogels from crosslinked cellulose nano/micro-fibrils and their fast shape recovery property in water, J Mater Chem, 22 (2012) 11642-11650.

[36] A.J. Onyianta, M. Dorris, R.L. Williams, Aqueous morpholine pre-treatment in cellulose nanofibril (CNF) production: comparison with carboxymethylation and TEMPO oxidisation pre-treatment methods, Cellulose, 25 (2018) 1047-1064.

[37] F.F. Lu, H.Y. Yu, C.F. Yan, J.M. Yao, Polylactic acid nanocomposite films with spherical nanocelluloses as efficient nucleation agents: effects on crystallization, mechanical and thermal properties, Rsc Adv, 6 (2016) 46008-46018.

[38] I.A. Udoetok, L.D. Wilson, J.V. Headley, "Pillaring Effects" in Cross-Linked Cellulose Biopolymers: A Study of Structure and Properties, Int J Polym Sci, 2018 (2018).

[39] A. Meftahi, R. Khajavi, A. Rashidi, M.K. Rahimi, A. Bahador, Preventing the collapse of 3D bacterial cellulose network via citric acid, J Nanostructure Chem, 8 (2018) 311-320.

[40] V.S. Raghuwanshi, U.M. Garusinghe, W. Batchelor, G. Garnier, Polyamide-amine-epichlorohydrin (PAE) induced TiO2 nanoparticles assembly in cellulose network, J Colloid Interf Sci, 575 (2020) 317-325.

[41] W. Li, S.F. Wang, W. Wang, C.R. Qin, M. Wu, Facile preparation of reactive hydrophobic cellulose nanofibril film for reducing water vapor permeability (WVP) in packaging applications, Cellulose, 26 (2019) 3271-3284.

[42] Y. Qing, R. Sabo, Y.Q. Wu, Z.Y. Cai, High-Performance Cellulose Nanofibril Composite Films, Bioresources, 7 (2012) 3064-3075.

[43] S. Sharma, Y.L. Deng, Dual Mechanism of Dry Strength Improvement of Cellulose Nanofibril Films by Polyamide-epichlorohydrin Resin Cross-Linking, Ind Eng Chem Res, 55 (2016) 11467-11474.

[44] P.T.Y. Beeran, V. Bobnar, S. Gorgieva, Y. Grohens, M. Finsgar, S. Thomas, V. Kokol, Mechanically strong, flexible and thermally stable graphene oxide/nanocellulosic films with enhanced dielectric properties (vol 6, pg 49138, 2016), Rsc Adv, 6 (2016) S7473-S7474.

[45] S. Ahola, M. Osterberg, J. Laine, Cellulose nanofibrils-adsorption with poly(amideamine) epichlorohydrin studied by QCM-D and application as a paper strength additive, Cellulose, 15 (2008) 303-314.

[46] C.L. Lv, Y.L. Su, Y.Q. Wang, X.L. Ma, Q. Sun, Z.Y. Jiang, Enhanced permeation performance of cellulose acetate ultrafiltration membrane by incorporation of Pluronic F127, J Membrane Sci, 294 (2007) 68-74.

[47] M.C. Yang, T.Y. Liu, The permeation performance of polyacrylonitrile/polyvinylidine fluoride blend membranes, J Membrane Sci, 226 (2003) 119-130.

[48] J.L. Lv, G.Q. Zhang, H.M. Zhang, F.L. Yang, Exploration of permeability and antifouling performance on modified cellulose acetate ultrafiltration membrane with cellulose nanocrystals, Carbohyd Polym, 174 (2017) 190-199.

[49] S.F. Anis, B.S. Lalia, R. Hashaikeh, Controlling swelling behavior of poly (vinyl) alcohol via networked cellulose and its application as a reverse osmosis membrane, Desalination, 336 (2014) 138-145.

[50] E.M.V. Hoek, A.K. Ghosh, X.F. Huang, M. Liong, J.I. Zink, Physical-chemical properties, separation performance, and fouling resistance of mixed-matrix ultrafiltration membranes, Desalination, 283 (2011) 89-99.

[51] Z.H. Wang, H.R. Yu, J.F. Xia, F.F. Zhang, F. Li, Y.Z. Xia, Y.H. Li, Novel GO-blended PVDF ultrafiltration membranes, Desalination, 299 (2012) 50-54.

838 [52] S.E. Keithley, S. Fakhreddine, K.A. Kinney, M.J. Kirisits, Effect of Treatment on the Quality
839 of Harvested Rainwater for Residential Systems, J Am Water Works Ass, 110 (2018) E1-E11.
840 [53] K. Li, S. Li, T.L. Huang, C.Z. Dong, J.W. Li, B. Zhao, S.J. Zhang, Chemical Cleaning of
841 Ultrafiltration Membrane Fouled by Humic Substances: Comparison between Hydrogen
842 Peroxide and Sodium Hypochlorite, Int J Env Res Pub He, 16 (2019).
843 [54] J.Q. Ding, S.L. Wang, P.C. Xie, Y.J. Zou, Y. Wan, Y.S. Chen, M.R. Wiesner, Chemical
844 cleaning of algae-fouled ultrafiltration (UF) membrane by sodium hypochlorite (NaClO):
845 Characterization of membrane and formation of halogenated by-products, J Membrane Sci,
846 598 (2020).
847 [55] Y.H. Shi, J.H. Huang, G.M. Zeng, Y.L. Gu, Y. Hu, B. Tang, J.X. Zhou, Y. Yang, L.X. Shi,
848 Evaluation of soluble microbial products (SMP) on membrane fouling in membrane
849 bioreactors (MBRs) at the fractional and overall level: a review, Rev Environ Sci Bio, 17 (2018)
850 71-85.
851 [56] X.W. Mao, P. Hadi, S. Lotfikatouli, B.J.S. Hsiao, H. Walker, Membrane bioreactors for
852 nitrogen removal from wastewater: A review., J Environ Eng, 146 (2020) 03120002.
853 [57] F. Mashayekhi, H. Hazrati, J. Shayegan, Fouling control mechanism by optimum ozone
854 addition in submerged membrane bioreactors treating synthetic wastewater, J Environ Chem
855 Eng, 6 (2018) 7294-7301.
856 [58] Y.F. Guan, C. Qian, W. Chen, B.C. Huang, Y.J. Wang, H.Q. Yu, Interaction between humic
857 acid and protein in membrane fouling process: A spectroscopic insight, Water Res, 145 (2018)
858 146-152.
859 [59] B. Zhang, S.L. Yu, Y.B. Zhu, Y. Shen, X. Gao, W.X. Shi, J.H. Tay, Efficiencies and
860 mechanisms of the chemical cleaning of fouled polytetrafluoroethylene (PTFE) membranes

during the microfiltration of alkali/surfactant/polymer flooding oilfield wastewater, Rsc Adv, 9 (2019) 36940-36950.

[60] J.X. Liu, B.Z. Dong, B.Q. Cao, D.S. Zhao, Z.H. Wang, Microfiltration process for surface water treatment: irreversible fouling identification and chemical cleaning, Rsc Adv, 6 (2016) 114005-114013.

[61] J.H. Kweon, J.H. Jung, S.R. Lee, H.W. Hui, Y. Shin, Y.H. Choi, Effects of consecutive chemical cleaning on membrane performance and surface properties of microfiltration, Desalination, 286 (2012) 324-331.

[62] A. Al-Amoudi, P. Williams, S. Mandale, R.W. Lovitt, Cleaning results of new and fouled nanofiltration membrane characterized by zeta potential and permeability, Sep Purif Technol, 54 (2007) 234-240.

[63] Y. Kakihana, L. Cheng, L.F. Fang, S.Y. Wang, S. Jeon, D. Saeki, S. Rajabzadeh, H. Matsuyama, Preparation of positively charged PVDF membranes with improved antibacterial activity by blending modification: Effect of change in membrane surface material properties, Colloid Surface A, 533 (2017) 133-139.

[64] A. Subramani, X.F. Huang, E.M.V. Hoek, Direct observation of bacterial deposition onto clean and organic-fouled polyamide membranes, J Colloid Interf Sci, 336 (2009) 13-20.

[65] A.W. Zularisam, A.F. Ismail, R. Salim, Behaviours of natural organic matter in membrane filtration for surface water treatment - a review, Desalination, 194 (2006) 211-231.

[66] K. Li, S. Li, Q. Su, G. Wen, T.L. Huang, Effects of Hydrogen Peroxide and Sodium Hypochlorite Aging on Properties and Performance of Polyethersulfone Ultrafiltration Membrane, Int J Env Res Pub He, 16 (2019).

[67] A. Venault, W.Y. Huang, S.W. Hsiao, A. Chinnathambi, S.A. Alharbi, H. Chen, J. Zheng, Y. Chang, Zwitterionic Modifications for Enhancing the Antifouling Properties of Poly(vinylidene fluoride) Membranes, Langmuir, 32 (2016) 4113-4124.

[68] B. Huang, H.K. Gu, K. Xiao, F.S. Qu, H.R. Yu, C.H. Wei, Fouling Mechanisms Analysis via Combined Fouling Models for Surface Water Ultrafiltration Process, Membranes-Basel, 10 (2020).

[69] H.Y. Ma, C. Burger, B.S. Hsiao, B. Chu, Fabrication and characterization of cellulose nanofiber based thin-film nanofibrous composite membranes, J Membrane Sci, 454 (2014) 272-282.

[70] S.N. Molnes, K.G. Paso, S. Strand, K. Syverud, The effects of pH, time and temperature on the stability and viscosity of cellulose nanocrystal (CNC) dispersions: implications for use in enhanced oil recovery, Cellulose, 24 (2017) 4479-4491.

[71] C.Y. Shao, H.L. Chang, M. Wang, F. Xu, J. Yang, High-Strength, Tough, and Self-Healing Nanocomposite Physical Hydrogels Based on the Synergistic Effects of Dynamic Hydrogen Bond and Dual Coordination Bonds, Acs Appl Mater Inter, 9 (2017) 28305-28318.

[72] L.Y. Li, F.X. Lu, C. Wang, F.L. Zhang, W.H. Liang, S. Kuga, Z.C. Dong, Y. Zhao, Y. Huang, M. Wu, Flexible double-cross-linked cellulose-based hydrogel and aerogel membrane for supercapacitor separator, J Mater Chem A, 6 (2018) 24468-24478.

Supporting Information

Nanostructured All-cellulose Membranes for Efficient Ultrafiltration of Wastewater

Mengying Yang[1], Sarah Lotfikatouli[2,4], Yvonne Chen[1], Tony Li[1],

Hongyang Ma[1,3], Xinwei Mao[2,4] and Benjamin S. Hsiao[1*]

[1] Department of Chemistry, Stony Brook University, Stony Brook, NY 11794, USA

[2] Department of Civil Engineering, Stony Brook, NY 11794, USA

[3] State Key Laboratory of Organic-Inorganic Composites, Beijing University of Chemical Technology, Beijing 100029, China

[4] New York State Center for Clean Water Technology, Stony Brook, NY 11794

[*]Corresponding Author: Tel: +1(631)632-7793, Fax: +1(631)632-6518, E-mail: Benjamin.Hsiao@stonybrook.edu

1. Morphology of CNF

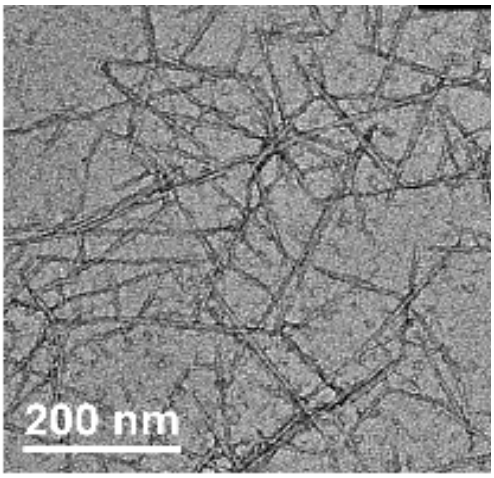

Fig. S1 TEM image of CNF with a degree of oxidation of 1.60 mmol/g.

2. Immersed Membrane Filtration System

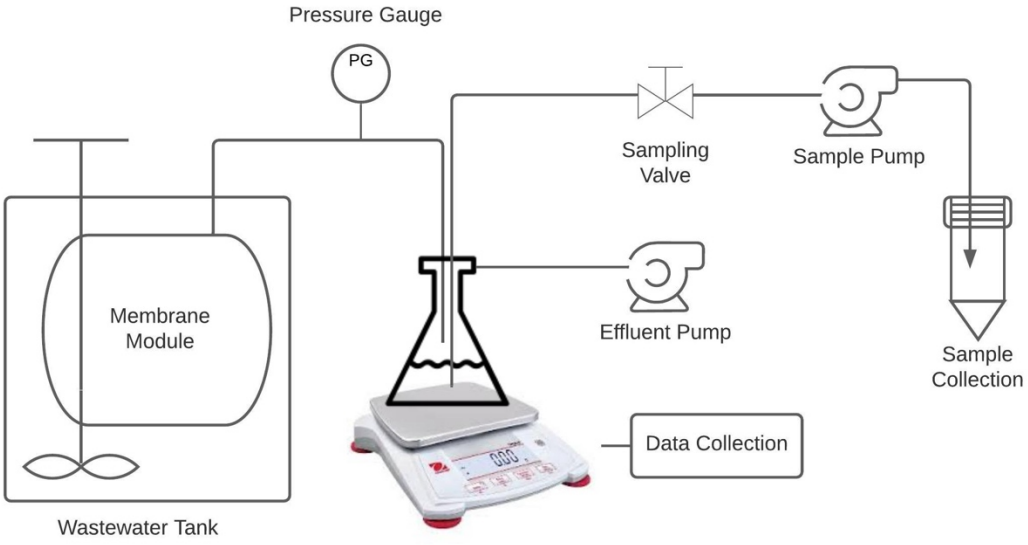

Fig. S2 Schematic diagram of the immersed membrane filtration system.

3. Zeta Potential of Lyocell, CNF, and Mixture Suspensions

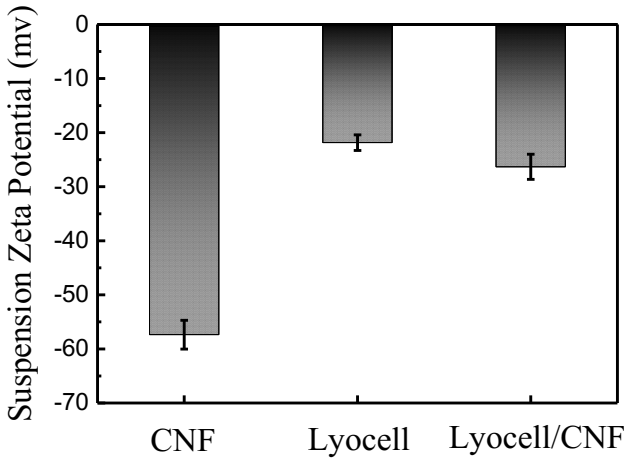

Fig. S3 Zeta potential data of CNF (0.15 wt%), lyocell (0.5 wt%), and lyocell/CNF mixture suspensions (50-0.85) at pH = 7.

4. Parameters of All-cellulose and Commercial Ultrafiltration Membranes

Table S1 The fouling mechanism study using combined fouling models at constant pressure.

Model	Expression	Fitted parameters
Cake filtration-complete blockage (CFCBM)	$V = \frac{J_0}{K_b}\left(1 - exp\left(\frac{-K_b}{K_c J_0^2}\left(\sqrt{1 + 2k_c J_0^2 t} - 1\right)\right)\right)$	K_c, K_b
Cake filtration-intermediate blockage (CFIBM)	$V = \frac{1}{K_i} ln\left(1 + \frac{K_i}{K_c J_0}\left(\sqrt{1 + 2K_c J_0^2 t} - 1\right)\right)$	K_c, K_i
Cake filtration-standard blockage (CFSBM)	$V = \frac{2}{K_s}\left(\beta cos\left(\frac{2\pi}{3} - \frac{1}{3} arccos(\alpha)\right) + \frac{1}{3}\right)$ $\alpha = \frac{8}{27\beta^3} + \frac{4K_s}{3\beta^3 K_c J_0} - \frac{4K_s^2 t}{3\beta^3 K_c}$ $\beta = \sqrt{\frac{4}{9} + \frac{4K_s}{3K_c J_0} + \frac{2K_s^2 t}{3K_c}}$	K_c, K_s

Table S2 Parameters of all-cellulose and commercial ultrafiltration membranes.

Series	PVDF-V6	PVDF-A6	PES-LX	All-cellulose
Target Feed	Industrial/ Wastewater	Industrial	Industrial	Wastewater+
MWCO/ Pore size	500 kDa	500 kDa	300 kDa	50 nm
Polymer	Modified PVDF	Conventional PVDF	Conventional PES	Lyocell/CNF
Water Permeation Flux (LMH/psi)	18.6 ± 2.2	10.6 ± 1.3	7.1 ± 1.3	8.8 ± 1.5
Zeta Potential (mV) at pH=7	5.5 ± 0.3	-20.4 ± 0.7	-10.1 ± 0.8	-16.1 ± 0.6
Contact Angle (°)	63.3 ± 1.5	72.3 ± 1.8	55.0 ± 3.6	~ 0

Table S3 The fitted parameters of different membranes using combined fouling models.

Membrane	Model	R^2	SSR	Fitted parameters
All-cellulose	CFCBM	0.9998	0.1214	K_c=1.9355, K_b=0.7869
	CFIBM	0.9862	12.935	K_c=0.4011, K_i=-0.0662
	CFSBM	0.8928	100.244	K_c=0.1465, K_s=1.64E-8
PVDF-V6	CFCBM	0.9994	0.5007	K_c=2.3503, K_b=0.6233
	CFIBM	0.9889	9.3449	K_c=0.4723, K_i=-0.0736
	CFSBM	0.8857	96.685	K_c=0.1665, K_s=1.5423E-5
PVDF-A6	CFCBM	0.9963	1.39	K_c=2.9657, K_b=1.9399
	CFIBM	0.9947	1.98	K_c=0.6991, K_i=-0.0766
	CFSBM	0.9375	23.60	K_c=0.3140, K_s=6.218E-5
PES-LX	CFCBM	0.9998	0.0441	K_c=11.7761, K_b=0.4067
	CFIBM	0.9847	3.0477	K_c=2.2219, K_i=-0.1636
	CFSBM	0.8674	26.350	K_c=0.7410, K_s=9.4514E-5